Advances in Aircraft System Identification at NASA Langley Research Center

Eugene A. Morelli* and Jared A. Grauer†
NASA Langley Research Center, Hampton, Virginia 23681

https://doi.org/10.2514/1.C037274

Advances in aircraft system identification at NASA Langley Research Center are discussed. The relevant time period includes the years since the last summary paper of this kind, which was published in the *Journal of Aircraft* in 2005. Research advances were achieved in flight test experiment design, frequency-domain modeling, real-time autonomous global modeling, rapid simulation development and updating, dynamic modeling in turbulence, flight data corrections, model uncertainty characterization, and aeroelastic modeling using distributed sensing. Possible future developments in the field are identified.

Nomenclature

a_x, a_y, a_z	=	body-axis accelerometer measurements, g
$\bar{c}$	=	wing mean aerodynamic chord, ft
$E[\bullet]$	=	expected value
f	=	frequency, Hz
j	=	imaginary number, $\sqrt{-1}$
max	=	maximum
min	=	minimum
p, q, r	=	body-axis roll, pitch, and yaw rates, rad/s or deg/s
$\bar{q}$	=	dynamic pressure, lbf/ft^2
$Re(\bullet)$	=	real part
rms	=	root mean square
T	=	maneuver length, s
V_o	=	nominal or reference true airspeed, ft/s
α	=	angle of attack, rad or deg
β	=	sideslip angle, rad or deg
$\delta_e, \delta_a, \delta_r$	=	elevator, aileron, and rudder deflections, rad or deg
$\mathbf{\Sigma}$	=	covariance matrix
ϕ, θ, ψ	=	Euler roll, pitch, and yaw angles, rad or deg
ω_E	=	engine speed, rev/min

Superscripts

T	=	transpose
-1	=	matrix inverse
$\hat{}$	=	estimate
$\cdot$	=	time derivative
$\sim$	=	Fourier transform
†	=	complex conjugate transpose

I. Introduction

AIRCRAFT system identification is the process of building mathematical models for aircraft based on experimental data. Research in this area has been conducted at NASA Langley Research Center (LaRC) in Hampton, Virginia, and at its predecessor organization, the NACA Langley Memorial Aeronautical Laboratory, since shortly after the invention of the airplane [1,2]. In 2005, a paper was published in a special issue of the *Journal of Aircraft* that included a summary of this history up to that time [2].

Received 2 November 2022; revision received 0 ; accepted for publication 17 December 2022; published online 6 April 2023.

*Research Engineer, Dynamic Systems and Control Branch, MS 308. Fellow AIAA.

†Research Engineer, Dynamic Systems and Control Branch, MS 308. Associate Fellow AIAA.

The present paper covers advances in aircraft system identification at NASA LaRC since 2005. The focus is on aircraft system identification from flight test data, although other relevant research in wind-tunnel testing and simulation development is also mentioned. Obtaining models from flight test data is important to 1) better understand and improve theoretical predictions and wind-tunnel test results, and 2) obtain accurate and comprehensive models for flight simulation, control system design, flying qualities assessment, stability and control characterization, and dynamic analysis.

In general, aircraft system identification research at NASA LaRC is motived by and related to NASA missions and NASA strategic research plans. Because of this, the work is not confined to routine applications of known aircraft system identification techniques to flight data from conventional vehicles, but rather involves the development of new techniques and approaches, along with their implementation and validation using flight test data from novel or concept-demonstration vehicles. Many different types of aerospace vehicles are used in NASA flight test applications, including hypersonic vehicles (X-43A, X-51A), subscale aircraft (S-2, T-2, Bat-4, E1), electric vertical take-off and landing (eVTOL) aircraft (LA-8), commuter aircraft (DHC-6), fighter jets (F-15B), trainer aircraft (MB-326M), space transportation vehicles (Ares I-X, Dream Chaser), and aeroelastic aircraft (X-56A). Examples are shown in Fig. 1.

These vehicles can experience large and/or fast changes in flight conditions or vehicle characteristics. Often, unusual flight conditions are of interest, including flight at high angles of attack or sideslip, poststall flight, spins, or rapid maneuvering. Complex phenomena are often encountered, such as unsteady and/or nonlinear aerodynamics, aeroelasticity, multibody dynamics, control interaction effects, and nonlinear dynamics. These challenges have driven the development and application of an extensive and versatile set of tools and techniques at NASA LaRC.

The next section reviews the methods and software tools used for aircraft system identification at NASA LaRC. The remainder of the paper is organized as a list of aircraft system identification flight test research efforts conducted by NASA LaRC since 2005, along with discussions of the associated achievements and their significance. Research advances were achieved in flight test experiment design, frequency-domain modeling, real-time autonomous global modeling, rapid simulation development and updating, dynamic modeling in turbulence, flight data corrections, model uncertainty characterization, and aeroelastic modeling using distributed sensing. Finally, projections for future developments in the field are given, along with a summary and conclusions.

II. Methods and Software Tools

To provide context for the research advances discussed later, this section gives a brief overview of the methods and software tools used for aircraft system identification at NASA LaRC.

Fig. 1 Selected NASA vehicles used for system identification flight research.

Figure 2 shows a high-level flowchart of the aircraft system identification process. At the beginning of the process, flight test experiment design combines prior information (e.g., from theoretical predictions, wind-tunnel tests, computational fluid dynamics, previous flight tests, etc.) with the purpose of the experiment to determine the flight conditions and control effectors to be used for the flight test. Prior information might also include aircraft mass/geometry properties and practical aspects of the aircraft flight control system and subsystems, such as control actuators and propulsion. Excitation inputs to be applied to the control effectors are designed to produce informative data for bare-airframe modeling while accounting for practical constraints such as control surface rate limits or flight test operational limits. Excitation inputs can also be applied at the pilot station or at various locations in a feedback control loop to achieve different modeling objectives.

The measured data are then analyzed for kinematic consistency in a data compatibility analysis. The purpose is to improve data accuracy

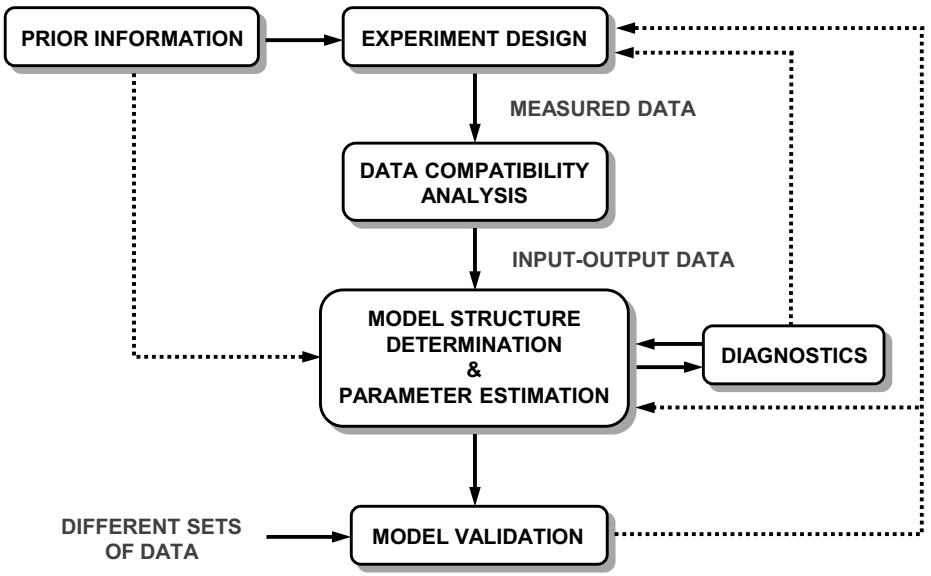

Fig. 2 Aircraft system identification flowchart, adapted from Ref. [2].

by identifying and removing any systematic instrumentation errors. These systematic errors are typically biases, scale factor errors, and relative time skews. The data might be transformed into the frequency domain using the finite Fourier transform, and sometimes processed further into frequency response data.

This is followed by determining an appropriate model structure based on the data information content and statistical modeling metrics and/or the objectives of the investigation. In some cases, the model structure is fixed for practical or theoretical reasons, such as the restriction to linear models for frequency responses or to a specified model structure for low-order equivalent system (LOES) modeling. Frequency response data displayed in a Bode plot are useful for linear model structure determination because of the relationship between straight-line approximations and the roots of transfer function numerators and denominators. For both linear and nonlinear models, stepwise regression and multivariate orthogonal function modeling can be applied in either the time domain or the frequency domain to determine the model structure. These techniques are based on the equation-error least-squares modeling formulation and employ a variety of statistical modeling metrics computed from the data.

The next step is statistical estimation of the unknown parameters in the selected model structure to achieve the best fit of the model to the measured data. The most commonly applied techniques are equation error (EE) and output error (OE), which are both maximum likelihood estimators under specific assumptions. Equation error generally results in the best match to derivative information in the equations of motion or to nondimensional aerodynamic coefficient data and has a closed-form analytical solution that is fast to compute. This technique involves only linear algebra and can be applied to one equation or to one nondimensional aerodynamic coefficient at a time using arbitrarily nonlinear model terms. The technique can be applied in practically any situation, including unstable aircraft operating under automatic feedback control, provided that the explanatory variables can be measured or estimated. Output error involves solving the model equations of motion to match measured response data, and requires an iterative, nonlinear optimization for the solution. This technique results in the best match to measured outputs and produces parameter estimates with favorable asymptotic properties, but also can be difficult to use and/or computationally expensive in some situations. Both techniques can be applied in the time domain using measured time series data or in the frequency domain using Fourier transform data or frequency response data.

A variety of diagnostics can be applied to evaluate the modeling results, including estimated model parameter uncertainties, signal-to-noise ratios for the measured response data, F ratios, coefficient of determination R^2, predicted squared error (PSE), and correlations among model terms and between candidate model terms and the data to be modeled. Estimated model parameters can be compared to theoretical predictions or results from wind-tunnel tests, or to flight test results from repeated or similar maneuvers. However, the most important evaluation of the modeling results is made by examining the predictive capability of the model using data that were not used to identify the model. This is the ultimate test of an identified model for its intended purpose, which is to predict the behavior of the physical system. Figure 2 also shows that the aircraft system identification process involves feedback and feedforward loops, as well as iteration. These are important aspects of effective aircraft system identification.

The range and diversity of aircraft system identification applications at NASA LaRC require an extensive and versatile set of tools to apply many different methods. A diverse toolset is important for cross-checking modeling results and for selecting the best approach for the problem at hand. This general philosophy was articulated by Gauss [3]:

> *It is always profitable to approach the more difficult problems in several ways, and not to despise the good although preferring the better.*

A software toolbox called System IDentification Programs for AirCraft (SIDPAC) has been developed and implemented in MATLAB® at NASA LaRC, starting in the early 1990s. SIDPAC now contains over 400 MATLAB files that implement a wide variety of techniques for aircraft system identification and related tasks. Many of these techniques were developed at NASA LaRC, but some are from the system identification and signal processing literature. SIDPAC also includes translations of legacy FORTRAN programs for aircraft system identification that were developed at NASA prior to the early 1990s. All programs in SIDPAC have been validated using both simulated and experimental data. SIDPAC includes a graphical user interface (GUI), as well as a realistic nonlinear F-16 simulation that can be flown in batch mode or piloted in real time using a personal computer and joystick. The F-16 nonlinear simulation provides a convenient way to generate realistic simulated flight test data for analysis and modeling.

SIDPAC is NASA software and is available through the NASA Software Catalog [4]. SIDPAC has been applied successfully to solve a wide variety of aircraft system identification problems at NASA LaRC and is used at more than 100 institutions worldwide. A comprehensive treatment of background, theory, and practical applications for aircraft system identification and SIDPAC is provided in a textbook originally published in 2006 [5], and currently available in a second edition [6]. The textbook [6] and SIDPAC software toolbox [4] are the basis for a graduate course in aircraft system identification taught at the National Institute of Aerospace (NIA) through the University of Maryland, and for a three-day professional short course that has been presented 30 times at various organizations in industry, government, and academia.

III. Research Topics

The sequence of research topics presented next is grouped according to topic rather than in chronological order. Details are omitted for brevity, but the cited references contain full descriptions of the methods and applications. Morelli and Klein [6] provide instructional material on aircraft system identification in general, as well as background information for the topics discussed next.

A. Flight Test Experiment Design

In 2002, a new flight test input design technique was developed at NASA LaRC [7,8], originally for application to the NASA X-43A hypersonic flight tests. This work was driven by the need to collect informative multi-axis flight data for dynamic modeling during a hypersonic flight test with rapidly changing flight conditions, strict limits for deviations from the planned flight trajectory, and very limited memory in the onboard flight computer. The excitation inputs that were developed as a solution and applied in flight, called orthogonal optimized multisine inputs, have important theoretical and practical advantages:

1) Multiple-input design capability for flight test efficiency, control interaction effects, and effective excitation of multi-axis aircraft dynamic responses

2) Mutual orthogonality in both the time and frequency domains, for flight test efficiency and high-accuracy modeling, regardless of whether the modeling is done in the time domain or the frequency domain

3) Wideband frequency content for all inputs, to provide robustness to deficiencies in knowledge of the aircraft dynamics prior to the flight test, and to enable the use of the same input design in many different flight conditions, and sometimes even for different aircraft

4) Balanced inputs optimized for minimum peak-to-peak amplitude of each multisine input with a selected power spectrum, to keep the aircraft response near the reference flight condition or flight trajectory, and to allow use of local linear model structures

5) Selectable power spectra to emphasize or de-emphasize excitation in specific frequency bands, and adjustable overall amplitude to account for variations in dynamic pressure and individual control effectiveness

For the orthogonal optimized multisine input design, each designed perturbation input is a sum of sinusoids with unique harmonic frequencies, optimized phase angles, and specified power distribution. The harmonic frequencies are selected to cover a

frequency range of interest. The wideband frequency content of the inputs is important because there is naturally some uncertainty in prior knowledge of the modal frequencies for the aircraft in flight, and wideband inputs provide robustness to that uncertainty. Phase shifts for the sinusoidal components of each input are optimized to achieve minimum peak-to-peak amplitude for the sum of sinusoids in each input. Amplitudes of the individual sinusoidal components for each input can be selected to achieve a specific power distribution with frequency. Typically, these excitation inputs are implemented using a flight control computer, by adding the inputs to the actuator commands, just before the rate and position limiting. This approach works very well even when a high-gain feedback control system is active [7–31]. Adding the excitation inputs to the pilot inputs can generate informative flight data for closed-loop modeling, such as LOES modeling. Adding the excitation inputs to control allocator/mixer inputs or to sensor outputs facilitates estimating stability margins. Orthogonal optimized multisine inputs can be injected at multiple places in the flight control system simultaneously to identify various dynamics based on data from a single flight test maneuver [31].

Complete details on how to design orthogonal optimized multisine inputs, along with related background information, can be found in Refs. [5–10]. A brief summary is given next. SIDPAC program `mkmsswp.m` can be used to design these inputs.

For the orthogonal optimized multisine input design, each multisine excitation input time series $\boldsymbol{u}$ is a sum of harmonic sinusoids with individual phase shifts ϕ_k:

$$\boldsymbol{u} = \sum_{k\in\{1,2,\ldots,M\}} A\sqrt{P_k}\sin\left(\frac{2\pi k\boldsymbol{t}}{T} + \phi_k\right) \tag{1}$$

where M is the total number of available harmonic frequencies, T is the time length of the excitation, A is the amplitude for the multisine input, P_k is the power fraction for the kth sinusoidal component, and $\boldsymbol{t}$ is the time vector. Each input is the sum of selected components from the pool of M harmonic sinusoids with frequencies

$$\omega_k = 2\pi k/T \qquad k = 1, 2, \ldots, M \tag{2}$$

The frequency $\omega_M = 2\pi M/T$ represents the upper limit of the frequency band for the excitation inputs, and $\omega_1 = 2\pi/T$ represents the lower limit. The interval $[\omega_1, \omega_M]$ rad/s specifies the range of frequencies where the aircraft dynamics are expected to lie. The frequency limits and the harmonic frequency assignments to individual inputs are selectable, so that the excitation can be implemented in a wide variety of ways for many practical flight test applications [10].

Each multisine input assembled using Eq. (1) will be applied to an individual control effector. The harmonic frequencies selected for each multisine input are unique to that input and are selected from a pool of available harmonic frequencies described by Eq. (2). Although harmonic frequency assignments can be made in many ways, a good practical approach is to assign the available harmonic frequencies alternately to the excitation inputs for the multiple control effectors, to achieve wideband frequency content for each excitation input. For a given frequency band of excitation, a longer excitation period T results in more harmonic frequencies to assign to the multiple inputs. The additional harmonic frequencies can be used to make the frequency content richer with more frequencies and finer frequency resolution for a given number of inputs, or to apply wideband frequency excitation for more inputs. This idea was used to successfully apply orthogonal optimized multisine inputs simultaneously to 16 individual controls on the T-2 subscale aircraft during a single 40-second flight test maneuver [9]. Of course, for a single input, all of the harmonic frequencies can be assigned to that one input.

Multisine inputs with unique harmonic frequencies are mutually orthogonal regardless of the phase angles ϕ_k. This means that the phase angles are free parameters that can be chosen without affecting the mutual orthogonality of the inputs. If the phase angles ϕ_k in Eq. (1) were chosen at random on the interval $(-\pi, \pi]$ rad, then, in general, the various harmonic components would add together at some points to produce a multisine input $\boldsymbol{u}$ with relatively large amplitude excursions. This is undesirable because such inputs can move the aircraft too far from the reference flight condition or flight trajectory. To prevent this, the phase angles ϕ_k for the harmonic components are optimized to minimize the relative peak factor (RPF), defined by

$$\mathrm{RPF}(\boldsymbol{u}) = \frac{[\max(\boldsymbol{u}) - \min(\boldsymbol{u})]/2}{\sqrt{2(\boldsymbol{u}^T\boldsymbol{u})/N}} = \frac{[\max(\boldsymbol{u}) - \min(\boldsymbol{u})]}{2\sqrt{2}\,\mathrm{rms}(\boldsymbol{u})} \tag{3}$$

Relative peak factor is a measure of the efficiency of an input for dynamic modeling purposes. For each multisine input $\boldsymbol{u}$ in Eq. (1), minimum RPF is achieved by adjusting the phase angles ϕ_k for the individual sinusoidal components of the input. The resulting optimization problem is nonconvex; however, a Nelder–Mead simplex algorithm can be applied to find a solution. Finally, the phase angles ϕ_k for the sinusoidal components in the multisine input are adjusted to time-shift the multisine input to begin and end at zero, thereby removing amplitude discontinuities at the endpoints. This is always possible because every sinusoidal component is a harmonic with base period equal to T seconds.

The sinusoidal components in Eq. (1) can be assigned arbitrary fractions of the total power in the multisine input by choosing the power fractions P_k, independently of the multisine amplitude A. The power fractions for the component sinusoids in each multisine input must sum to 1:

$$\sum_k P_k = 1 \tag{4a}$$

To achieve a uniform power distribution, P_k are selected as

$$P_k = \frac{1}{n} \tag{4b}$$

where n is the number of sinusoidal components included in the summation of Eq. (1). Each input $\boldsymbol{u}$ can have arbitrary amplitude A, subject to practical flight test and modeling considerations, such as load limits and collecting data appropriate for a linear model structure, among others. Power fractions for the individual sinusoidal components of a multisine input can be changed to concentrate input excitation power at frequencies where dynamic modes are likely or expected, or to avoid exciting unwanted dynamic response such as fuel slosh or structural modes, or to improve dynamic excitation by assigning frequency content according to capabilities of individual control effectors or actuators. In the absence of such knowledge, a good approach is to implement uniform power distribution according to Eq. (4b).

Figure 3 shows an example of an orthogonal optimized multisine input design for a fixed-wing airplane with three control effectors and $T = 10$ s. The vertical lines in Fig. 3a show the frequencies assigned to each individual excitation input, with the height indicating the power fraction P_k at each frequency. In this example, the power was concentrated near 1 Hz for elevator and rudder, based on prior information, but the inputs still retained wideband frequency content. For the aileron, the power was distributed evenly across the frequency band, reflecting no prior information. In the frequency domain, the inputs are mutually orthogonal because of their interleaved frequencies, or unique frequency content. The inputs are also mutually orthogonal in the time domain, because harmonic sinusoids with different harmonic numbers are mutually orthogonal in the time domain, regardless of phase shifts [5–10]. The multiple input time series for this orthogonal multisine input design with optimized phase angles are shown in Fig. 3b. This input design was flown on the T-2 subscale aircraft and resulted in excellent multi-axis modeling results.

The mutual orthogonality of the inputs allows simultaneous application of multiple inputs, for flight-test efficiency and practical utility, because a large amount of multiple-input energy can be injected into the aircraft rapidly at a selected flight condition that may not be sustainable for a long time. In addition, mutually orthogonal excitation inputs decorrelate the control position data, provide rich

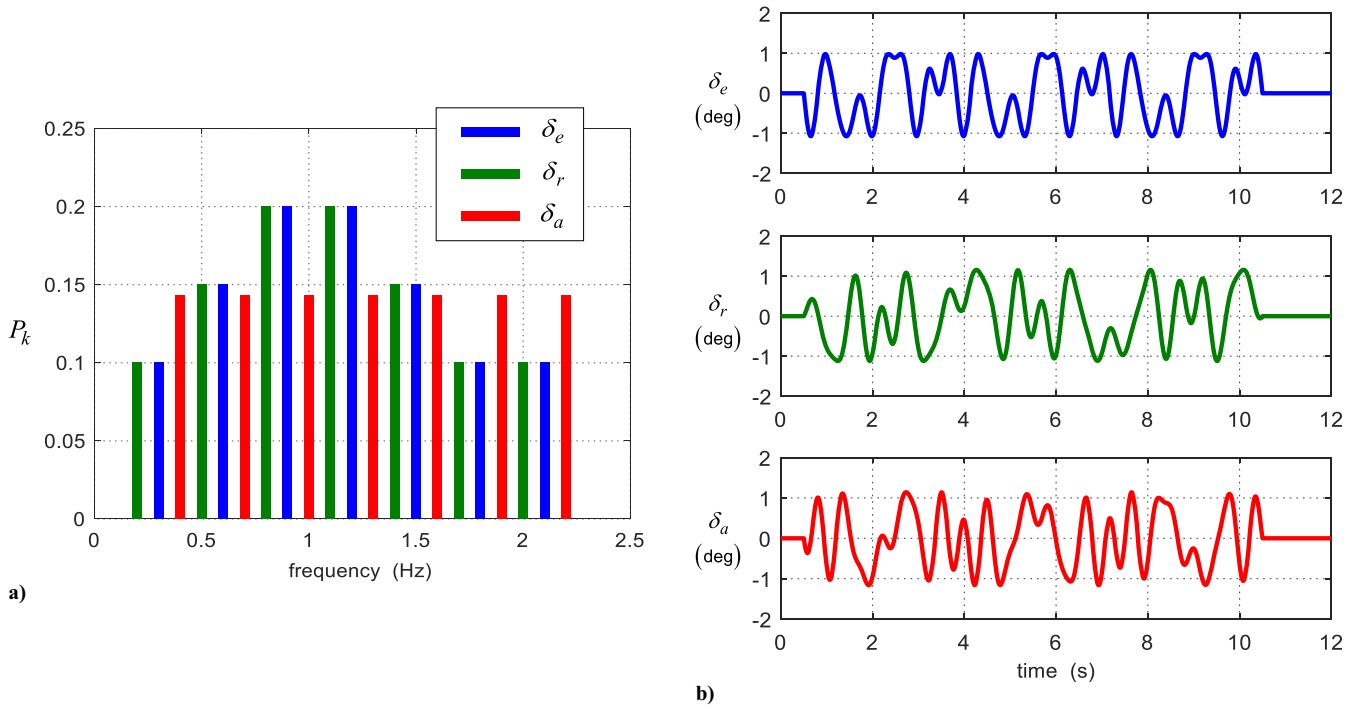

Fig. 3 Orthogonal optimized multisine inputs: a) spectra; b) time series.

data information for control interaction effects, and effectively excite multi-axis response over a wide frequency band, all of which lead to more accurate modeling. These advantages are present regardless of whether the modeling is done in the time or frequency domains, because the input orthogonality is present in both domains.

In practice, pilot inputs, automated guidance, and/or active feedback control can act to spoil the orthogonality (zero pairwise correlations) of a multiple-input design. However, good modeling results require only low correlations, not zero correlations, so that slightly correlated inputs still work well in practice. The arrangement shown in Fig. 4 has been used very successfully in a wide variety of flight test applications with high-gain active feedback control, including hypersonic vehicle stability and control [8,11–14], stability and control for open-loop unstable fighter aircraft [7,15,16], real-time global modeling [26–28], and real-time modeling for an aeroelastic aircraft [29,30].

The injection point for multiple excitation inputs is important when flight testing aircraft with active feedback control. For bare airframe modeling, the injection point must be after the control system and before the control command rate and position limiters, as shown in Fig. 4. Using this approach, the control system only senses the effects of the excitation inputs on the aircraft response through the feedback of measured outputs, and has no other knowledge of the excitation inputs. Because the effects of the excitation inputs on the aircraft measured outputs are delayed by the aircraft dynamics, the control system cannot completely extinguish the excitation inputs, and some of the excitation input energy gets through to the aircraft. The general idea is to inject perfectly uncorrelated (orthogonal) excitation inputs, so that any correlations caused by the pilot, guidance system, and/or feedback control will be at levels lower than the practical upper limit of 0.9 in absolute value [5,6]. Accurate bare-airframe modeling results can then be obtained using a variety of methods [5,6], based on the flight data collected with active feedback control.

In the years since 2005, the orthogonal optimized multisine input design technique has been successfully applied in many flight tests. This input design is now standard practice at NASA LaRC, mainly due to its practicality, effectiveness, and efficiency, compared to conventional single-axis input designs, such as doublets, multistep inputs such as the 3-2-1-1, and frequency sweeps. An important practical characteristic is the ability to use these inputs at a wide variety of flight conditions to rapidly inject energy on multiple inputs simultaneously without causing the aircraft to depart from the reference flight condition or flight trajectory. This is the result of the wideband frequency content and phase optimization that minimizes the input amplitudes for specified input power spectra. Furthermore, a sum of harmonic sinusoids over the base period for the input design will always have balanced input energy above and below zero, which keeps the aircraft response near the reference flight condition or flight trajectory. This provides the versatile and effective capability to collect highly informative multi-axis data at any point in a flight test by simply activating the multisine excitations. Test pilot workload is reduced to flying the aircraft to the desired flight condition, then

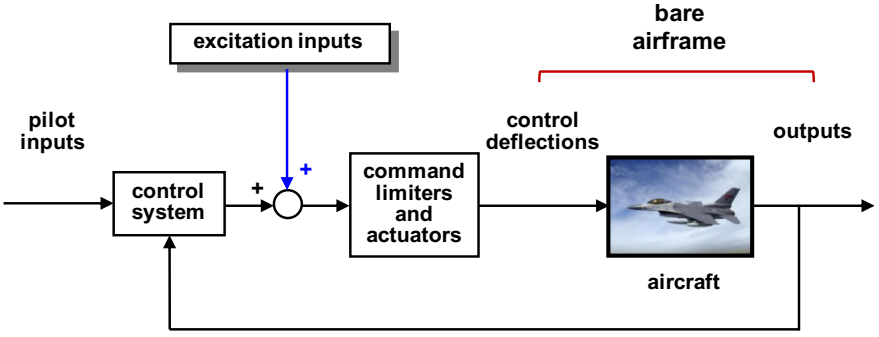

Fig. 4 Injecting excitation inputs for an aircraft flying with active feedback control.

activating the multisine inputs with a switch or pushbutton. This avoids pilot training on how to implement effective excitation inputs and reduces test pilot skill requirements. In addition, the inputs are easy to design using SIDPAC software.

Successful flight test applications and research advances enabled by the orthogonal optimized multisine input design include hypersonic stability and control flight tests on the X-43A [8,11,12] and X-51A [13,14]; supersonic stability and control flight tests on a modified F-15B fighter aircraft [7,15,16]; and real-time modeling in turbulence [17], real-time modeling without air flow angle measurements [18], and dynamic modeling for flight data with unknown time skews [19] on the T-2 subscale aircraft. Other successful flight test applications include real-time modeling for airframe icing envelope protection on the DHC-6 Twin Otter commuter aircraft [20–22]; stability and control flight testing in both nominal and unusual flight conditions [9,10,23–25] and global aerodynamic modeling from flight data [9,23–28] on the S-2, T-2, Bat-4, Woodstock, and E1 subscale aircraft; and estimating the separate effects of pitch rate and angle-of-attack rate on the T-2 subscale aircraft [32]. Orthogonal optimized multisine inputs were also successfully applied in flight for real-time frequency response estimation [30,33–36] and output-error modeling using frequency responses [37,38] on the T-2 and X-56A subscale aircraft; real-time fault detection on the T-2 subscale aircraft [39]; aeroelastic modeling on the X-56A subscale aircraft [29,40–42]; determining aircraft moments of inertia from flight test data on the E1 subscale aircraft [43]; stability and control flight testing during approach to landing on the Dream Chaser space vehicle [44]; and dynamic modeling during ascent on the Ares 1-X space launch vehicle [45–47]. Additional information on the orthogonal optimized multisine input design method can be found in publications on optimal input design [48] and practical frequency domain methods [49]. Orthogonal optimized multisine inputs can provide effective and efficient multi-axis excitation to collect informative flight data for dynamic modeling in a wide variety of flight tests.

Multisine time series have other uses as well. Based on the observation by Lanczos [50] that random noise can be represented as a multisine with random phase angles, a method was developed to synthesize random noise with precise power spectra that can be specified [51]. Comparisons with standard random number generators indicated that multisines could produce white noise sequences of higher quality with respect to several statistical metrics [51,52]. This approach can also be used to emulate in-flight turbulence with specific power spectra by applying multisine inputs to control surfaces while flying in calm air [53], or to generate tracking targets for pilot modeling [54].

Another important advance in flight test experiment design was the continuous application of orthogonal optimized multisine inputs while the pilot flew slowly through a range of flight conditions, as opposed to applying the excitations at a single nominal flight condition. This approach is very practical for global nonlinear aerodynamic modeling, because the pilot workload is reduced to flying the aircraft slowly through various flight conditions, while automated orthogonal optimized multisine inputs excite multi-axis aircraft response near the time-varying flight condition. This fills the multivariate explanatory variable hyperspace with informative flight data that have low correlations [6,9,23–28], which is required for accurate global nonlinear aerodynamic modeling.

Figure 5 shows flight data from a global maneuver on the T-2 subscale aircraft, where the pilot flew a slow approach to stall and through recovery, while the orthogonal optimized multisine inputs were executed simultaneously by the flight control computer. This procedure collected highly informative multi-axis flight data over a large range of angle of attack in a single efficient flight test maneuver. The plots in Fig. 5a show the aircraft responses and control deflections, resulting from pilot inputs for a slow change in flight condition from nominal cruise flight through stall and recovery, with simultaneous automated orthogonal optimized multisine input excitations. The cross plots in Fig. 5b on the right show examples of the resultant excellent coverage in explanatory variable space with uncorrelated data. These plots are two-dimensional projections of the data coverage in multidimensional explanatory variable hyperspace. Other two-dimensional projections were similar.

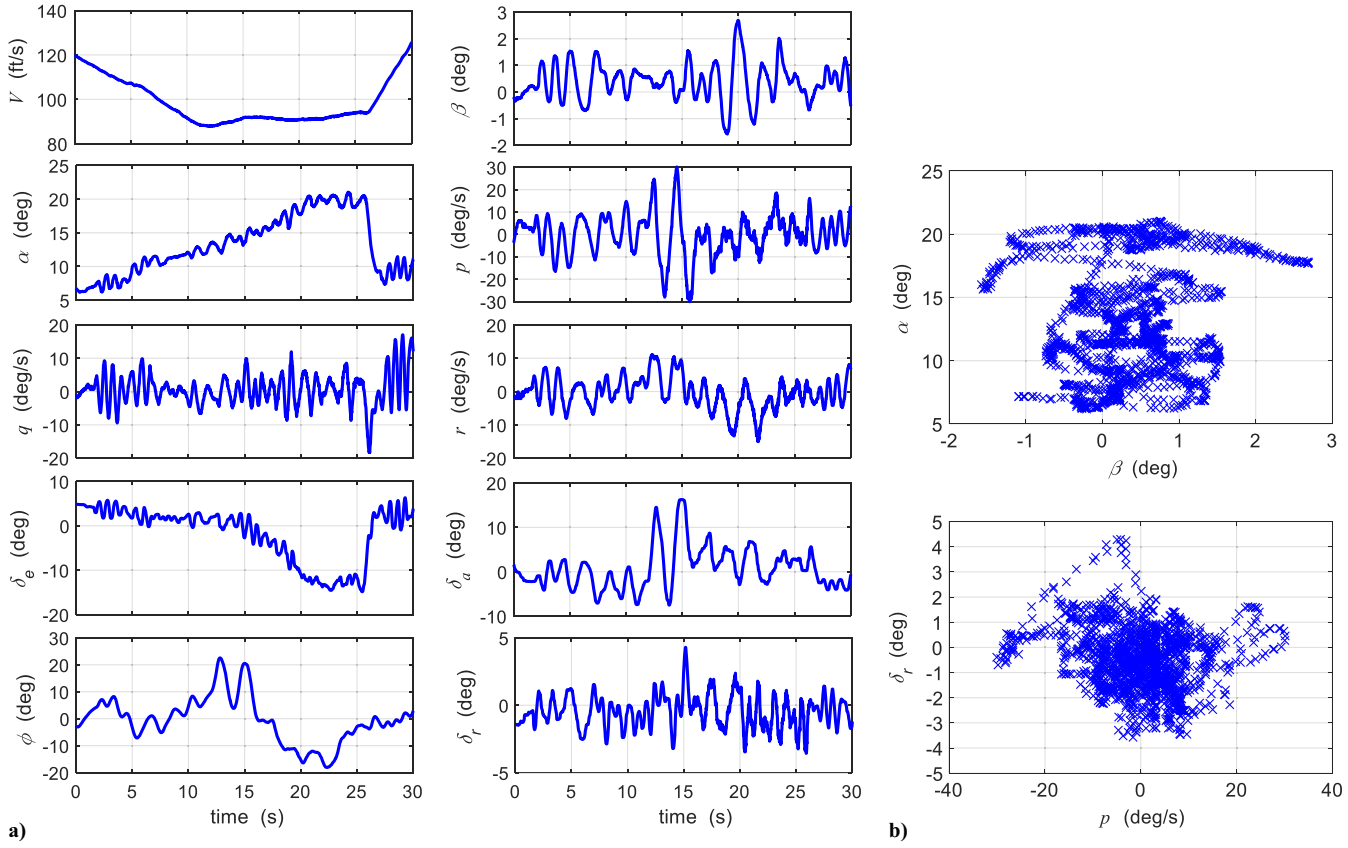

Fig. 5 Global flight test maneuver: a) measured time series; b) selected explanatory data subspace coverage.

Further investigations showed that test pilots can implement very good approximations to orthogonal optimized multisine inputs [55–58]. These inputs are called uncorrelated pilot inputs (UPI). For bare-airframe modeling, UPI only work for aircraft without feedback control, whereas automated orthogonal optimized multisine inputs can be used effectively for bare airframe modeling regardless of whether feedback control is active or not. Either UPI or orthogonal optimized multisine inputs can be applied to the pilot controls for closed-loop modeling, regardless of the feedback control.

Several test pilots demonstrated the ability to fly effective UPI both at individual flight conditions and while maneuvering the aircraft slowly through a wide range of flight conditions [55–58]. Test pilots from NASA LaRC and the National Test Pilot School (NTPS) demonstrated this ability in the MB-326M Impala jet trainer aircraft, which had no feedback control, and completely reversible flight control with pushrods connecting the pilot stick and rudder pedals with the elevator, ailerons, and rudder. The only pilot training for the flight tests was detailed discussions at preflight briefings [58]. Figure 6 shows flight data from a global maneuver flown by a test pilot over large ranges of Mach number, angle of attack, normal load factor, and dynamic pressure, with simultaneous multi-axis UPI applied. In addition, random step changes to the commanded power level were made to achieve decorrelated inputs for modeling thrust and thrust-induced aerodynamic effects [58].

This flight test technique provided rich data information content for global modeling over a large portion of the flight envelope in a single efficient piloted maneuver. Three or four inputs are probably the practical upper limit for a pilot implementing UPI, whereas an automated system can implement an arbitrary number of excitation inputs accurately and simultaneously.

Cross plots of the control surface deflections during a 27-second UPI flight test maneuver flown on the Impala aircraft are shown in Fig. 7. The pilot moved the controls in an uncorrelated fashion over the desired range of control surface deflections. Pairwise correlations

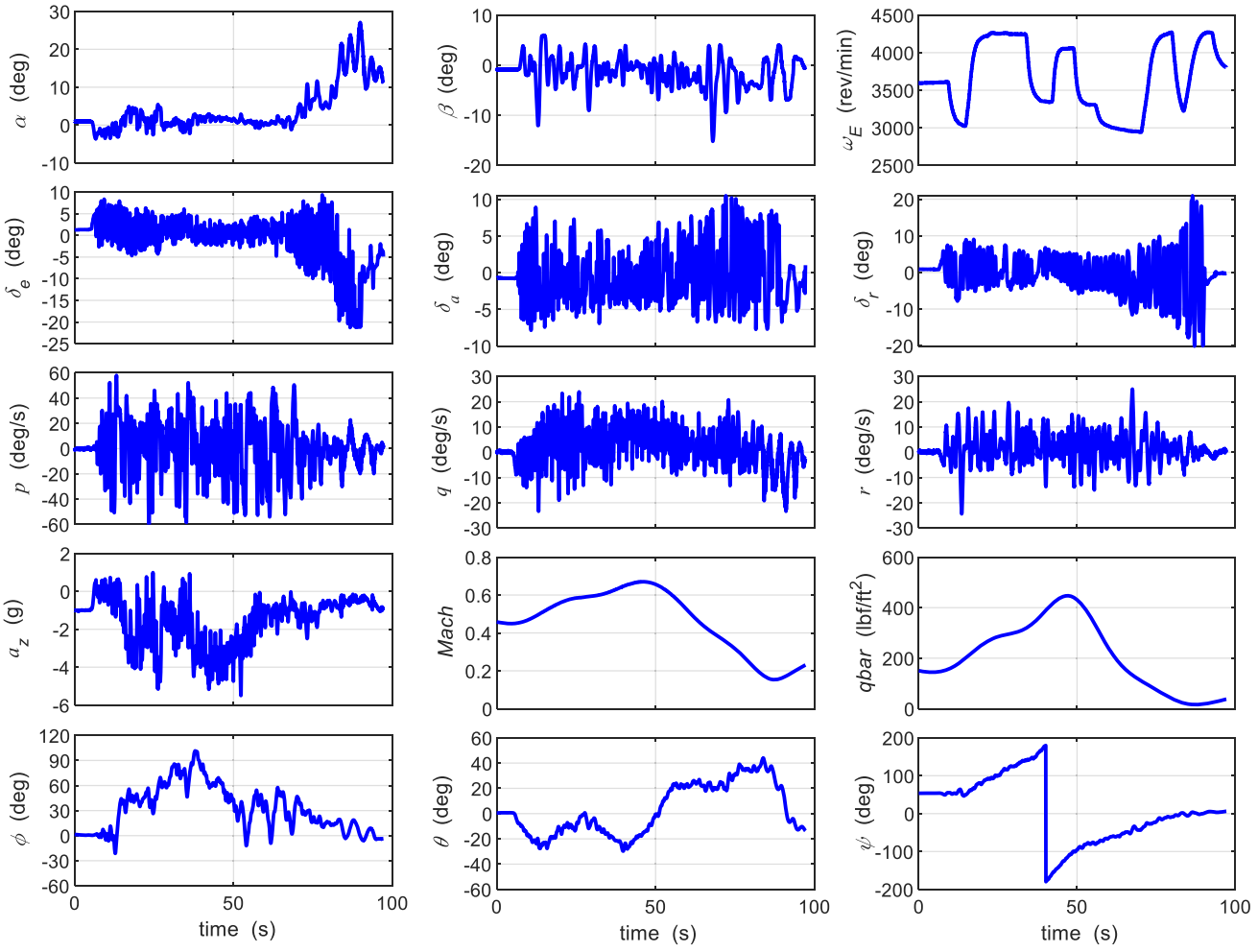

Fig. 6 Piloted global flight test maneuver using uncorrelated pilot inputs (UPI).

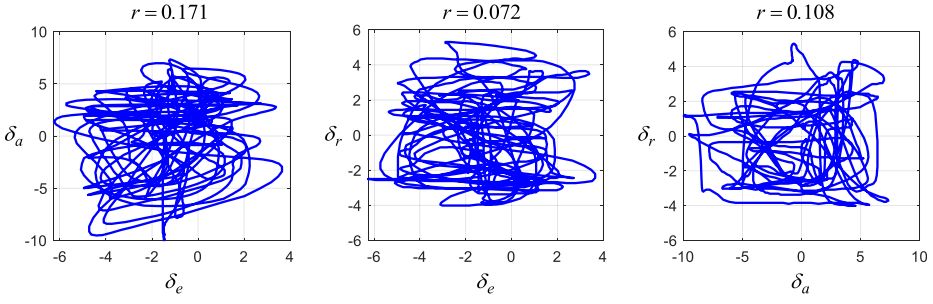

Fig. 7 Cross plots of control surface deflection data for uncorrelated pilot inputs (UPI).

(r) for the control surface deflections were less than 0.2 in absolute value, as indicated on the plots. Although these inputs were not orthogonal (pairwise correlations were not equal to zero), the pairwise correlations achieved by the pilot were very low and easily low enough for excellent local and global modeling results, which typically require absolute pairwise correlations less than 0.9.

B. Frequency-Domain Modeling

A seminal paper written by Vladislav Klein at NASA LaRC in 1978 [59] developed and explained aircraft modeling in the frequency domain using equation-error and output-error methods with either Fourier transform data or frequency response data. Many frequency-domain modeling techniques in current use, including some implemented in SIDPAC, have origins in that paper. Frequency-domain modeling has many advantages, such as providing particular types of physical insight, applicability to common control-system design methods and flying qualities analysis, robustness to noise, simple and effective approaches for data smoothing, and more efficient calculations for model parameter estimation, among others [5,6,49,59–67].

Since 2005, aircraft system identification research at NASA Langley has included a strong focus on frequency-domain methods, mainly because of their practicality and applicability to real-time modeling. Significant advances have been made in developing and applying frequency-domain methods using equation-error and output-error methods with high-resolution Fourier transform data in a partial frequency band, as well as output-error methods with frequency response data obtained accurately and efficiently using orthogonal optimized multisine inputs. Real-time calculation of both Fourier transform data and frequency response data have been important for these developments. A detailed summary of practical frequency-domain techniques developed and used at NASA LaRC can be found in Ref. [49]. The material in this section provides an overview with flight test applications, along with references that can be consulted for more detailed information.

The basis for frequency-domain methods is the finite Fourier transform, which is the analytical tool used to transform time-domain data to the frequency domain. The finite Fourier transform of a time series $x(t)$ is defined as

$$\tilde{x}(\omega) \equiv \int_0^T x(t)e^{-j\omega t}\,\mathrm{d}t \qquad \omega = 2\pi f \tag{5}$$

The finite Fourier transform $\tilde{x}(\omega)$ can be interpreted as a coefficient in an expansion of $x(t)$ in terms of basis functions $e^{-j\omega t} = \cos\omega t - j\sin\omega t$ for various analysis frequencies ω, or as a measure of the similarity of $x(t)$ to the function $e^{-j\omega t}$. There is considerable freedom in the choice for the analysis frequency ω, and this fact can be used advantageously in practice.

When $x(t)$ is sampled at discrete times separated by a constant time interval Δt, the finite Fourier transform can be approximated by

$$\tilde{x}(\omega) \approx \Delta t \sum_{i=0}^{N-1} x(i)e^{-j\omega i\Delta t} \tag{6}$$

where the time length of the measured data is $T = (N-1)\Delta t$ and

$$t_i = i\Delta t \quad x(i) \equiv x(t_i) = x(i\Delta t) \qquad i = 0, 1, 2, \ldots, N-1 \tag{7}$$

The summation in Eq. (6) is called the discrete Fourier transform (DFT), denoted by $X(\omega)$:

$$X(\omega) \equiv \sum_{i=0}^{N-1} x(i)e^{-j\omega i\Delta t} \tag{8}$$

The DFT can be computed recursively for an analysis frequency ω by implementing the summation in Eq. (8) as a running sum. The DFT at sample time $i\Delta t$ is related to its value at time $(i-1)\Delta t$ by

$$X_i(\omega) = X_{i-1}(\omega) + x(i)e^{-j\omega i\Delta t} \tag{9a}$$

where

$$e^{-j\omega i\Delta t} = e^{-j\omega\Delta t}e^{-j\omega(i-1)\Delta t} \tag{9b}$$

The quantity $e^{-j\omega\Delta t}$ is a constant for a given frequency ω and constant sampling interval Δt. It follows that the DFT can be computed recursively for a given frequency at each time step using one addition in Eq. (9a) and two multiplications—one in Eq. (9b) using the stored constant $e^{-j\omega\Delta t}$ for frequency ω and one in Eq. (9a). There is no need to store the time-domain data in memory when computing the DFT in this way, because each sampled data point is processed immediately as a projection onto Fourier basis functions. In this sense, the recursive DFT acts as a compact frequency-domain memory for the information in the data. Information from additional time-domain data can be stored in the frequency domain without increasing memory requirements. Furthermore, the DFT is available at any time $i\Delta t$. The approximation to the finite Fourier transform is completed using Eq. (6):

$$\tilde{x}(\omega, t_i) \approx \Delta t X_i(\omega) \tag{10}$$

The recursive DFT in Eq. (9a) implements data information memory for as long as the running sum is continued. When the situation changes, older data should be discounted or forgotten in some way. If this is not done, then the speed of response to changes is progressively degraded, as new information must overwhelm an increasingly longer memory. Consequently, there is a tradeoff between the desired rapid response to changes versus retaining enough information for accurate modeling.

The simplicity of Eq. (9a) and the linearity of the Fourier transform with respect to the time series data $x(i)$ allow easy implementation of data forgetting in the recursive DFT, by modifying Eq. (9a) to

$$X_i(\omega) = \lambda X_{i-1}(\omega) + x(i)e^{-j\omega i\Delta t} \tag{11}$$

This can be interpreted as multiplying each past value of the time series by a forgetting factor λ, where $0 < \lambda < 1$, at each time step. Old data are gradually devalued and eventually discarded for practical purposes. Applying a constant forgetting factor in this way corresponds to exponential data forgetting with respect to time [6]. Partial forgetting can be implemented by subtracting saved values of the running sums at earlier times. Alternatively, the recursive DFT can be simply restarted by setting all $X(\omega)$ values to zero (complete forgetting) based on an event, such as a flight condition change, the start of a new maneuver, a change in the aircraft configuration, or the detection of some type of failure or damage.

1. *Frequency-Domain Equation-Error Modeling Using Fourier Transform Data*

Equation-error parameter estimation can be applied in the frequency domain using an approach similar to equation-error parameter estimation in the time domain, except that Fourier transform data are used instead of measured time-domain data [5,6,49,59,61–63]. At NASA LaRC, an equation-error modeling approach was developed based on choosing the Fourier transform frequencies with high resolution in a partial frequency band, instead of using default frequencies typically used in fast Fourier transform (FFT) algorithms. This approach provides important practical and computational advantages, including automatic data smoothing, fast computation because the number of selected analysis frequencies is relatively small regardless of the maneuver time length, and accurate parameter estimates with valid uncertainty measures from simple calculations [5,6,49,62,63]. The approach automatically removes wideband noise on the regressors in the frequency domain, which avoids the bias errors typically associated with equation-error methods [6,49,62]. Equation-error modeling in the frequency domain is a regression formulation with complex numbers, which has a closed-form optimal solution. Applying equation-error modeling in the frequency domain with closely spaced analysis frequencies in a frequency band where the aircraft dynamics are expected is a

practical, simple, and fast modeling approach that produces model parameter accuracy comparable to what can be obtained using iterative nonlinear optimization in a time-domain output-error formulation [62].

The first step for equation-error modeling in the frequency domain is to apply the finite Fourier transform in a partial frequency band corresponding to the dynamics of interest. This automatically smooths the data by rejecting noise outside the bandwidth of interest, and makes the resulting equation-error parameter estimates practically unbiased [6,62]. Analysis frequencies for a 20-second dynamic maneuver on a full-scale aircraft might be

$$\boldsymbol{f} = \begin{bmatrix} 0.100 & 0.125 & \dots & 1.475 & 1.500 \end{bmatrix}^T \text{ Hz} \qquad \boldsymbol{\omega} = 2\pi \boldsymbol{f} \tag{12}$$

The lower bound is chosen as $2/T$, where T is the time length of the maneuver, so that the lowest analysis frequency will have two complete cycles in T seconds. The upper bound is chosen to include the dynamics of interest, typically identified as the upper bound of the frequency range for large components relative to the noise level in the frequency domain. This upper limit can be readily found by transforming the data into the frequency domain for a wide frequency band first (easily accomplished with the SIDPAC `fint.m` program) to determine the upper bound of the frequency band where the large components lie.

In the frequency domain, the set of overdetermined equations resulting from equation-error modeling has the same form as in the time domain, except that the number of data points is M, where M is the number of selected frequencies for the Fourier transformation, and the problem now involves complex numbers [5,6]. For example, an equation-error modeling problem for the nondimensional pitching moment coefficient C_m can be formulated as

$$\tilde{z} = \tilde{\boldsymbol{X}}\boldsymbol{\theta} + \tilde{\boldsymbol{\varepsilon}} \tag{13}$$

where

$\tilde{z} = \begin{bmatrix} \tilde{C}_m(1) & \tilde{C}_m(2) & \dots & \tilde{C}_m(M) \end{bmatrix}^T = M \times 1$ vector of Fourier transform values for the response

$\tilde{\boldsymbol{X}} = \begin{bmatrix} \tilde{\alpha} & \frac{\tilde{q}\bar{c}}{2V_o} & \tilde{\delta}_e \end{bmatrix} = M \times 3$ matrix of Fourier transform values for the modeling functions or regressors

$\boldsymbol{\theta} = \begin{bmatrix} C_{m_\alpha} & C_{m_q} & C_{m_{\delta_e}} \end{bmatrix}^T = 3 \times 1$ vector of unknown parameters

$\tilde{\boldsymbol{\varepsilon}} = \begin{bmatrix} \tilde{\varepsilon}(1) & \tilde{\varepsilon}(2) & \dots & \tilde{\varepsilon}(M) \end{bmatrix}^T = M \times 1$ vector of Fourier transform values for the equation errors

The matrix $\tilde{\boldsymbol{X}}$ is assembled using Fourier transform data, with each column representing a modeling function, also called a regressor. The best estimate of $\boldsymbol{\theta}$ in a least-squares sense comes from minimizing the sum of squared differences between the transformed response measurements $\tilde{z}$ and the model output $\tilde{y} = \tilde{\boldsymbol{X}}\boldsymbol{\theta}$:

$$J(\boldsymbol{\theta}) = \frac{1}{2}(\tilde{z} - \tilde{\boldsymbol{X}}\boldsymbol{\theta})^{\dagger}(\tilde{z} - \tilde{\boldsymbol{X}}\boldsymbol{\theta}) \tag{14}$$

The least-squares solution for the unknown parameter vector θ is [5,6]

$$\hat{\boldsymbol{\theta}} = [Re(\tilde{\boldsymbol{X}}^{\dagger}\tilde{\boldsymbol{X}})]^{-1} Re(\tilde{\boldsymbol{X}}^{\dagger}\tilde{z}) \tag{15}$$

and the estimated model output is

$$\hat{\tilde{\boldsymbol{y}}} = \tilde{\boldsymbol{X}}\hat{\boldsymbol{\theta}} \tag{16}$$

The estimated parameter covariance matrix is computed from [5,6,49]

$$\boldsymbol{\Sigma}(\hat{\boldsymbol{\theta}}) \equiv E[(\hat{\boldsymbol{\theta}} - \boldsymbol{\theta})(\hat{\boldsymbol{\theta}} - \boldsymbol{\theta})^T] = \hat{\tilde{\sigma}}^2 [Re(\tilde{\boldsymbol{X}}^{\dagger}\tilde{\boldsymbol{X}})]^{-1} \tag{17}$$

$$\hat{\tilde{\sigma}}^2 = \frac{1}{2T} Re\Big[(\tilde{z} - \hat{\tilde{\boldsymbol{y}}})^{\dagger}(\tilde{z} - \hat{\tilde{\boldsymbol{y}}})\Big] / [\max(\boldsymbol{f}) - \min(\boldsymbol{f})] \tag{18}$$

The standard errors of the estimated parameters are given by the square root of the diagonal elements of the covariance matrix:

$$s(\hat{\theta}_j) = \sqrt{\Sigma_{jj}} \qquad j = 1, 2, \dots, n_p \tag{19}$$

where n_p is the number of unknown parameters, so that $n_p = 3$ for the example. The noise variance expression in Eq. (18) is needed when the analysis frequencies are chosen in a partial frequency band, instead of over the entire frequency range $[0, f_N]$ Hz, where $f_N = 1/(2\Delta t)$ is the Nyquist frequency. Frequency resolution can be selected as $\Delta f = 1/T$ or finer, but a frequency resolution more coarse than $1/T$ will omit frequency content [5,6,49].

There is no bias term in the frequency-domain model (e.g., no C_{m_o} in the example), because the time series data are detrended prior to applying the Fourier transform, to avoid leakage from low-frequency components such as biases and linear trends with time [5,6,49]. For the recursive DFT, detrending can be done in real time using high-pass filtering [5,6,49,63].

As is true for other equation-error formulations, this approach can be applied separately to individual degrees of freedom or dynamic equations, and works well even for open-loop unstable aircraft operating under closed-loop feedback control [5,6,9,11–16,25–29]. The equation-error formulation using Fourier transform data weights modeling errors in the real and imaginary parts of the complex frequency-domain data equally [5,6,49].

The recursive Fourier transform with high-resolution analysis frequencies selected in a partial frequency band can be combined with equation-error parameter estimation to achieve real-time modeling in a practical, efficient algorithm, as first described in [63]. Because the recursive Fourier transform provides frequency-domain data at every time step, the least-squares parameter estimation and uncertainty calculations can be executed at any time to provide real-time modeling results. However, these calculations can typically be done at a slower rate, such as 2 Hz, because the model parameters typically do not change rapidly, except in cases of extreme maneuvering, damage, or failures. Furthermore, significant differences in the modeling results require substantial changes in the data information, which require at least a short time interval of informative flight data. Executing the computations in Eqs. (15–19) at every time step would waste valuable onboard computing resources.

The accurate real-time parameter estimates and valid real-time uncertainty measures produced with this approach are particularly important for applications such as efficient flight testing in steady or time-varying flight conditions, robust control, dynamic analysis, accident investigation, and fault detection. This innovation has been used successfully in many flight test applications, including real-time simulator validation [9], real-time dynamic modeling in turbulence [17], and real-time modeling without air flow angle measurements [18] on the T-2 subscale aircraft; real-time detection of in-flight icing on the DHC-6 Twin Otter [20–22]; real-time modeling in unusual and time-varying flight conditions on the S-2, T-2, Bat-4, Woodstock, and E1 subscale aircraft [9,23–28]; and real-time aeroelastic modeling on the X-56A aircraft [29].

The frequency-domain equation-error modeling approach was combined with frequency-domain time skew estimation and applied in postflight analysis to achieve accurate stability and control modeling from flight data with unknown time skews [19]. Model structure determination in the frequency domain using both linear and nonlinear candidate model terms was also developed and applied to flight test data [6,64]. Nonlinear terms in a frequency-domain equation-error modeling formulation require some additional data conditioning, and modeling metrics are slightly different in the frequency

domain, but otherwise, the same model structure determination methods developed and used successfully in the time domain can be applied in the frequency domain [6,49,64].

2. *Frequency Response Estimation Using Orthogonal Optimized Multisine Inputs*

At NASA LaRC, orthogonal optimized multisine inputs have been combined with the recursive Fourier transform to estimate multiple-input, multiple-output frequency responses simultaneously in real time. The motivations for this work include monitoring stability margins and detecting faults in flight, improving flight test efficiency, assessing flying qualities, and gaining insight into the model structure for high-order linear models.

In general, the frequency response is the ratio of the Fourier transform of a single output y to the Fourier transform of a single input u:

$$\hat{H}(\omega) = \frac{\tilde{y}(\omega)}{\tilde{u}(\omega)} \tag{20}$$

In some applications, this simple expression has been used with long-term sinusoidal inputs (sine dwells), one frequency at a time, to estimate the frequency response of single-input, single-output dynamic systems. Although such testing is not practical or efficient for aircraft, multiple orthogonal optimized multisine inputs can be applied effectively using this concept, as explained next.

Orthogonal optimized multisine inputs have frequency content that is discrete and known prior to the analysis. The dominant frequency content in the output is then known to lie at the designed discrete input frequencies, assuming linear system dynamics, which is inherent in the use of frequency responses. This greatly simplifies the calculation of frequency responses, because frequency response values can be computed directly at the discrete frequencies where input power is known to exist, using the discrete Fourier transform and the simple expression in Eq. (20) [6,30,31,34–39,49]. Furthermore, because the discrete Fourier transform can be computed recursively, as discussed earlier, the same approach can be applied to estimate frequency responses in real time [30,34–36,39]. Prior to this work, a time-domain method for frequency response estimation using multisine inputs was developed [33]. Real-time frequency response estimation was also demonstrated for multiple inputs and multiple outputs in wind-tunnel testing [65].

Frequency response estimation errors occur because of the nonlinearity inherent in all aircraft, which produces distortion and spectral content in the output at frequencies other than the input frequencies. However, this error is present in any case when using frequency responses, which can characterize only linear relationships. Another source of error is leakage due to the finite data record length, but these errors are relatively small for detrended time-domain data, and can be minimized or eliminated completely with careful design of the multisine inputs and the data record length [49].

Figure 8 shows an example of real-time frequency response estimation using flight test data from the T-2 aircraft. Only the elevator to pitch rate frequency response is shown, although orthogonal optimized multisine excitations at different frequencies were simultaneously applied to the aileron and rudder controls. A first-order, high-pass filter with corner frequency at 0.47 rad/s (0.075 Hz) was used to detrend the data in real time, and the recursive Fourier transform and frequency response were computed using Eqs. (9a) and (20). Figure 8a shows the frequency response estimates obtained at the end of the maneuver, using all of the data, as dots. For comparison, the corresponding frequency response for a short-period dynamic model estimated using output-error parameter estimation with Fourier transform data [5,6,49,59] is shown as a solid line. Figure 8b shows the evolution of the real-time frequency-response estimates at 1 s intervals, with the output-error result at the end of the maneuver. This example demonstrates the accuracy of the simple real-time frequency response estimation that is possible using orthogonal optimized multisine inputs. More information and an additional example can be found in Refs. [34–36].

Orthogonal optimized multisine inputs can be applied to multiple controls at the same time, so that many frequency responses can be extracted simultaneously. This improves flight test efficiency, resulting in time and cost savings. As noted in Ref. [67], Eq. (20) only produces the correct result for open-loop systems or when evaluating broken-loop responses for stability margins. However, this approach can be extended to estimate open-loop frequency responses from closed-loop data using the joint input–output (JIO) technique [30,31,67].

Orthogonal optimized multisine inputs must be implemented by a computer. A pilot can approximate these inputs effectively for accurate dynamic modeling in the time domain or using frequency-domain methods based on Fourier transform data, as described earlier. However, for frequency response estimation, piloted approximation of orthogonal optimized multisine inputs induces continual transient response, which degrades the spectral estimation results [57].

Significant advances were made to estimate open-loop and closed-loop frequency responses in real time using orthogonal optimized multisine inputs [30,33–36]. Important applications include output-error bare-airframe modeling using frequency responses estimated

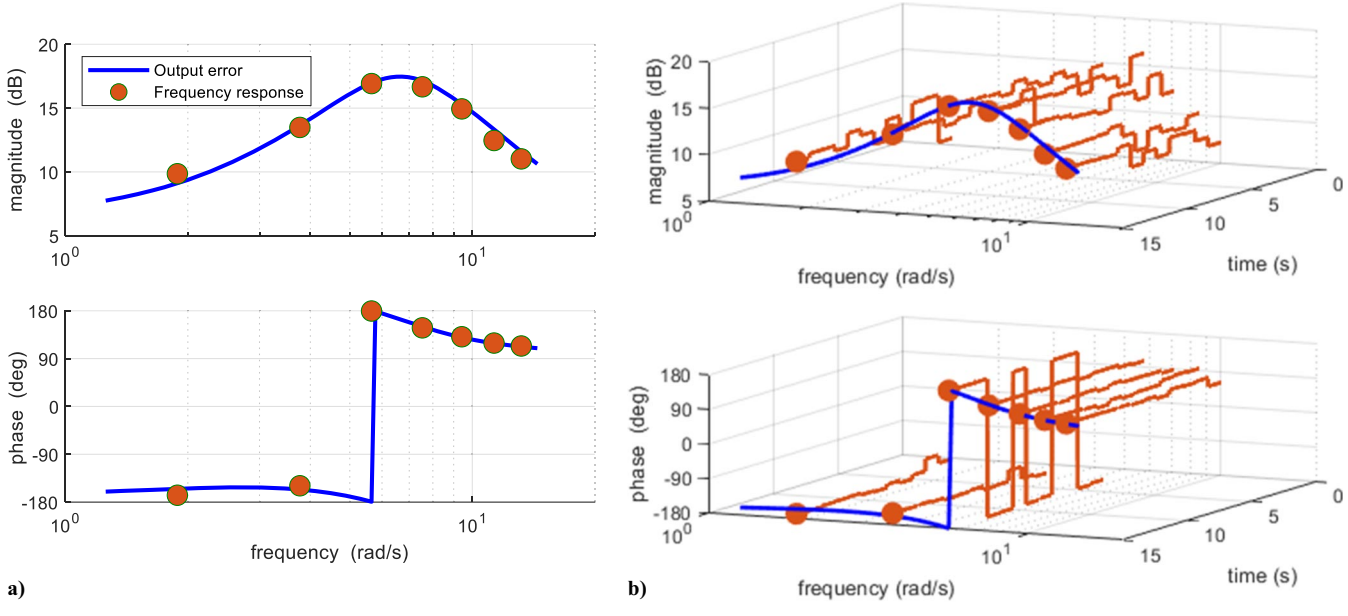

Fig. 8 Real-time frequency response estimation: a) final result; b) time evolution.

from closed-loop flight testing on the T-2 and X-56A aircraft [37,38]; multiple simultaneous frequency responses for various feedback control loops using multipoint injection of orthogonal optimized multisine excitation inputs on the T-2 and X-56A aircraft [31]; real-time fault detection for the T-2 aircraft [39]; and aeroelastic modeling for the X-56A aircraft [40–42].

C. Real-Time Autonomous Global Modeling

Real-time autonomous global modeling is a game-changing capability and is an important component of the aircraft system identification research at NASA LaRC. The vision is an aircraft with onboard intelligence to autonomously learn its own global aerodynamics in real time based on flight data alone, without assistance or guidance from a human analyst. This capability can save significant time and money in flight testing, simulation development, and control system design, and makes it possible for an aircraft to autonomously develop and maintain an onboard model specific to its own characteristics and flight experience. This contrasts with the conventional assumption that the results from flight testing a particular airframe can be used for all other airframes of the same design, regardless of manufacturing variations or operational history. Practical applications for real-time autonomous global modeling include robust adaptive control, efficient flight testing, and real-time fault or degradation detection, as well as rapid aircraft design evaluation, development, and simulation.

Research toward achieving real-time autonomous global modeling has been pursued at NASA LaRC for more than a decade, as depicted in Fig. 9. The evolution began with autonomous time-domain global nonlinear modeling in batch mode on the ground using orthogonal optimized multisine inputs applied in time-varying and unusual flight conditions during flight tests in 2009–2012 [9,25]. This was followed in 2013–2014 by onboard global nonlinear modeling in batch mode using multivariate orthogonal function modeling and fuzzy logic modeling. Global and local maneuvers were developed and flown by test pilots applying UPI on the Impala jet trainer [55,58]. In 2015, autonomous global nonlinear modeling was achieved in real time on the ground with telemetered data using multivariate orthogonal function modeling and orthogonal optimized multisine inputs [26]. This work introduced real-time orthogonalization and autonomous model structure determination for both linear and arbitrarily nonlinear model terms. Real-time autonomous global nonlinear modeling was achieved onboard the aircraft in the NASA Learn-to-Fly project with the Woodstock and E1 aircraft [27]. This capability was a critical component in the successful flight test demonstration of the Learn-to-Fly concept [68].

An alternate approach combined real-time local linear models estimated using the recursive Fourier transform and equation-error parameter estimation in the frequency domain to form a global model for the E1 aircraft [28]. This approach was extended by applying multivariate orthogonal function modeling to local linear model parameters to identify a global aeropropulsive model from wind-tunnel data for an urban air mobility vehicle [69]. Research and development efforts for the important real-time autonomous global modeling technical capability are continuing at NASA LaRC, with applications to more complex aircraft configurations with more control effectors and significant interaction effects among the explanatory variables.

D. Rapid Simulation Development and Updating

An important application of autonomous global nonlinear modeling is rapid development of flight simulations directly from flight test data. This concept was applied using flight test data from the Impala jet trainer aircraft and the T-2 and E1 subscale aircraft.

In a related simulation study [56], piloted global maneuvers with UPI were used to collect data for global nonlinear aerodynamic modeling to accurately characterize aircraft behavior near stall. Multivariate orthogonal function modeling [5,6] was applied in the time domain using spline functions to accurately model aerodynamic nonlinearity near stall. This work demonstrated that a few piloted global maneuvers flown on a transport aircraft could be used to collect informative data for accurate global modeling, including the regions near stall. The modeling results can be used to build accurate simulations for pilot training in stall recognition and safe recovery, and can also be applied to augment existing simulators to include accurate nonlinear aerodynamics near stall and poststall.

Multivariate orthogonal function modeling was also applied to several wind-tunnel databases to identify a generic global nondimensional aerodynamic model structure that can be used to simulate different aircraft [70]. Using the identified generic global model structure, global aerodynamic models for eight different aircraft can be implemented in a nonlinear simulation by simply changing the values of 45 model parameters in the generic aerodynamic model structure.

Many simulations are based on aerodynamic and propulsion databases implemented in tables of values obtained from wind-tunnel tests and ground-based propulsion tests, and/or from computational methods. This could be considered as a distributed-parameter model with the values in the tables being the many distributed parameters. In contrast, modeling results from a flight test maneuver typically consist of relatively few lumped model parameters that represent the maneuver data, such as the parameters in a linear dynamic model. This disparity is the root of the difficulty in updating an existing simulation database using flight test data.

If the information in the simulation database can be converted to a model form similar to flight test models, then the information in both the simulation database and the flight data can be combined. This idea was applied in the time domain to update simulations using flight test

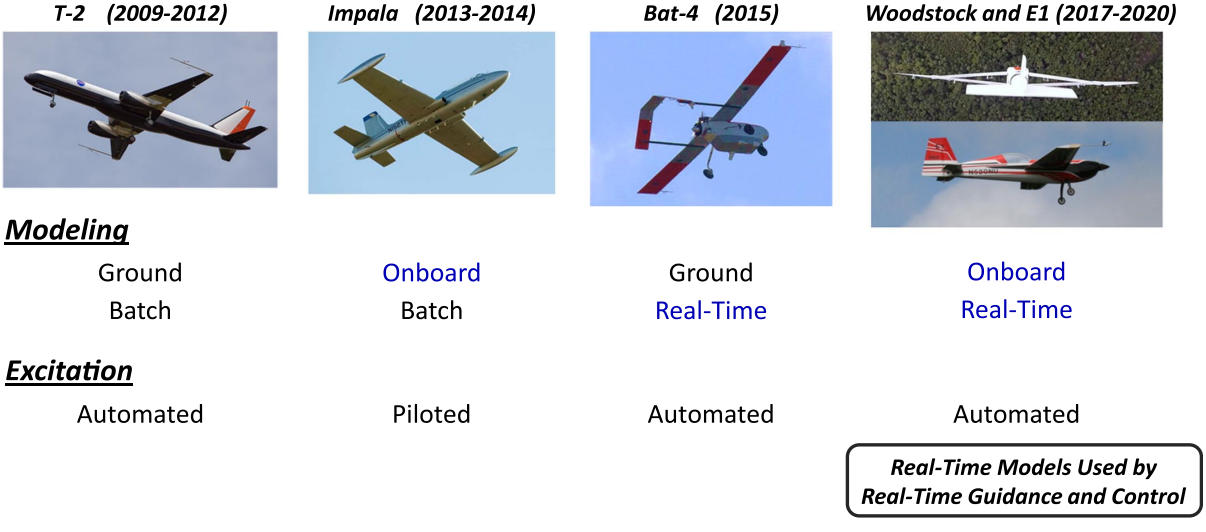

Fig. 9 Evolution of real-time autonomous global modeling at NASA LaRC.

data [71]. The existing simulation database was modeled locally using only the tabular values that would be needed to simulate the flight test maneuver. This modeling was done with a multivariate orthogonal function modeling technique [5,6], resulting in a local parametric model with associated model parameter uncertainties. The model can then be updated using the measured flight data in a Bayesian modeling formulation [5,6,71,72].

An analogous approach was developed using frequency-domain modeling for the flight data update step in a Bayesian approach [64]. This provided advantages in computational efficiency, robustness to noise, and enhanced ability to model unsteady effects. In addition, an approach was developed to identify nonlinear model terms in the frequency domain and to use those terms in the frequency-domain update step [64].

Regardless of whether the updating was done in the time domain or frequency domain, the result was a local response surface model that represented the flight update. The final step was to update the existing simulation database. The flight update was considered as a local model increment that must be blended into the surrounding existing database, in order to avoid discontinuities in the updated simulation database. The local flight test increment model was faded to zero at the boundaries of the flight data update region, which can be done effectively with Gaussian blending functions [64,71,72].

The final result is an updated simulation database that combines the information in both the simulation database and the flight data to produce an accurate flight-updated simulation. The procedure is carried out autonomously based on data information content and statistical modeling error measures, and does not require human analyst judgment.

E. Dynamic Modeling in Turbulence

Dynamic modeling in turbulence is difficult because turbulence is typically an unmeasured input. However, practical methods for dynamic modeling in turbulence are valuable for efficient flight testing and real-time modeling in all flight conditions. For those reasons, the problem was studied at NASA LaRC.

1. *Dominating the Turbulence*

One approach for dynamic modeling in turbulence is to apply excitation inputs with amplitudes large enough so that the response to the excitation inputs dominates the unknown effects of the turbulence. This approach was successfully demonstrated in flight with the subscale T-2 aircraft, which is significantly affected by turbulence, due to its small size [17]. However, this approach has the disadvantage that the excitation amplitudes must be increasingly large as the turbulence level increases. In practice, excitation amplitudes are limited for reasons such as flight safety, load and control position limits, and keeping the aircraft response within the range of validity for a given model structure.

2. *Sifting*

Assuming that the aircraft response can be accurately characterized with a linear model structure, the response to known multisine excitation inputs will be composed of sinusoids at the same frequencies, but with different magnitudes and phase angles. Analytic forms for these sinusoidal responses can be used to sift the deterministic response of the aircraft to the known multisine excitations from the measured response [17]. However, the accuracy of this approach is limited by the fact that turbulence also produces some response at the multisine excitation frequencies. This effect can be mitigated with larger excitation input amplitudes, as in the previous approach.

3. *Turbulence Measurement or Reconstruction*

Another approach to the problem is to measure or reconstruct the turbulence from other data, thereby converting the unknown turbulence inputs into known inputs, then applying parameter estimation techniques as usual. This works well if the turbulence inputs can be measured or reconstructed accurately [73,74].

In Ref. [74], an approach for reconstructing turbulence from sensor measurements, originally developed at the NACA Langley Aeronautical Laboratory in the 1950s, was extended and improved upon using more accurate analyses. Figure 10a shows the turbulence power spectra for the vertical gust component reconstructed from flights of the T-2 aircraft in various levels of turbulence. The roll-off with increasing frequency in this plot is similar to the Dryden turbulence model. Reconstructed turbulence inputs were used in an equation-error formulation with Fourier transform data to estimate stability and control derivatives. An interesting result was that the presence of moderate and severe turbulence helped to decorrelate the pitch rate and angle-of-attack rate derivatives (e.g., C_{m_q} and $C_{m_{\dot{\alpha}}}$), which are normally highly correlated without special maneuvers [32]. Parameter estimation results for pitching moment stability and control derivatives in various levels of turbulence are shown in Fig. 10b. Scatter in the estimates for a given level of turbulence is attributed to

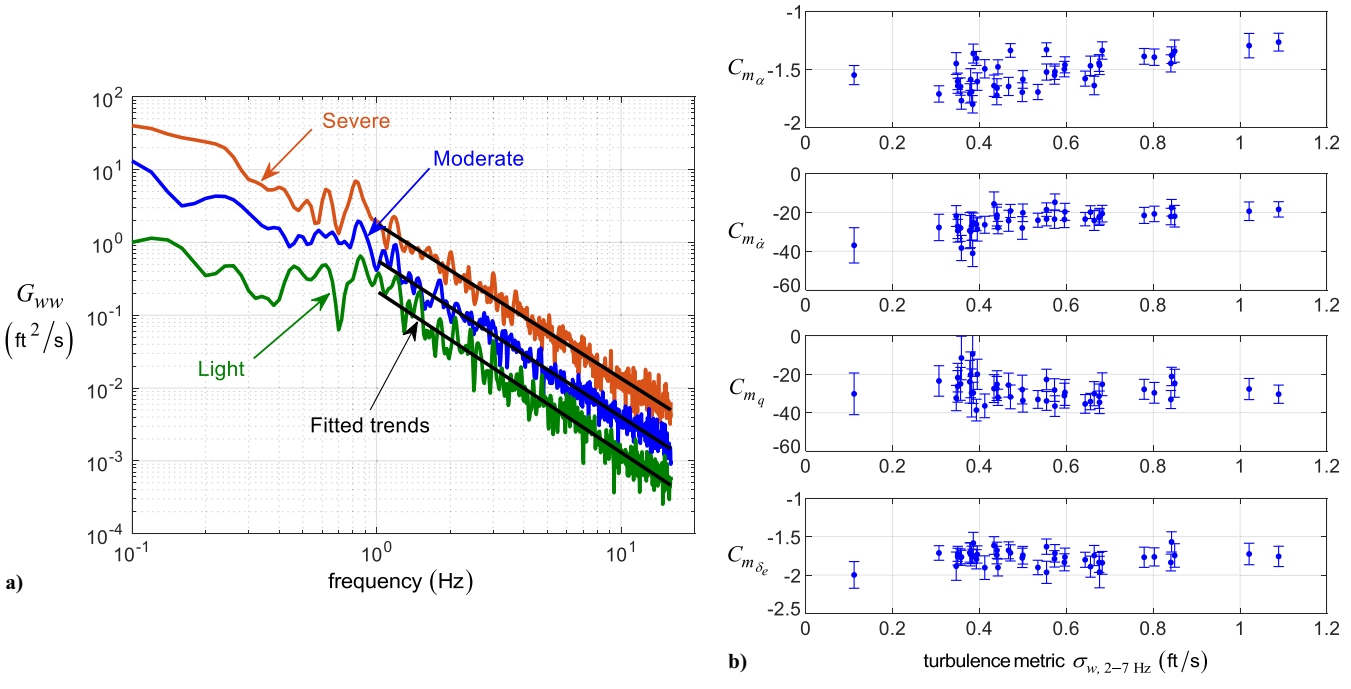

Fig. 10 T-2 aircraft in turbulence: a) reconstructed turbulence spectra; b) parameter estimates.

unsteady aerodynamics that were not modeled, different flight test conditions, the random nature of turbulence, and small time skews in the measurements.

4. Filter Error Parameter Estimation

A general approach to dynamic modeling in turbulence is to include noise in the dynamic model equations to represent the turbulence, then estimate quantities that characterize the turbulence amplitudes and power spectra. The resulting parameter estimation problem formulation is called the filter error method [5,6,75]. Filter error is a maximum likelihood parameter estimation method that includes both process noise (noise in the dynamic model equations) and measurement noise (noise in the output equations). Process noise in the dynamic model equations means that the states are stochastic quantities that must be estimated, typically using a Kalman filter. In contrast, the equation-error method ignores measurement noise but includes process noise, whereas the output-error method ignores process noise but includes measurements noise. The filter-error method is therefore more general, but also more difficult to apply in practice, due to problems such as increased complexity, more unknown parameters, issues with convergence and identifiability, and others [5,6,75].

A new formulation of the filter-error problem, along with a practical and accurate solution was developed at NASA LaRC [76]. The method uses a signal processing technique called global optimal Fourier smoothing [5,6,77] to accurately estimate the measurement noise variance separately from the filter-error optimization. This reduces the number of unknowns in the filter-error optimization. Afterward, an optimization procedure is used to minimize the maximum likelihood cost function for the unknown model parameters (e.g., stability and control derivatives) and the unknown process noise covariance matrix [76].

The approach has been successfully applied to flight path reconstruction, data compatibility analysis, and parameter estimation in turbulence [76,78]. For example, Fig. 11 shows flight data from the T-2 aircraft flying in severe turbulence when orthogonal optimized multisines were applied to the elevator, aileron, and rudder.

The model fit to the flight data using filter error with a longitudinal short-period dynamic model is also shown. Analysis of repeated maneuvers flown in various levels of turbulence showed consistent parameter estimation results using this filter-error approach [76].

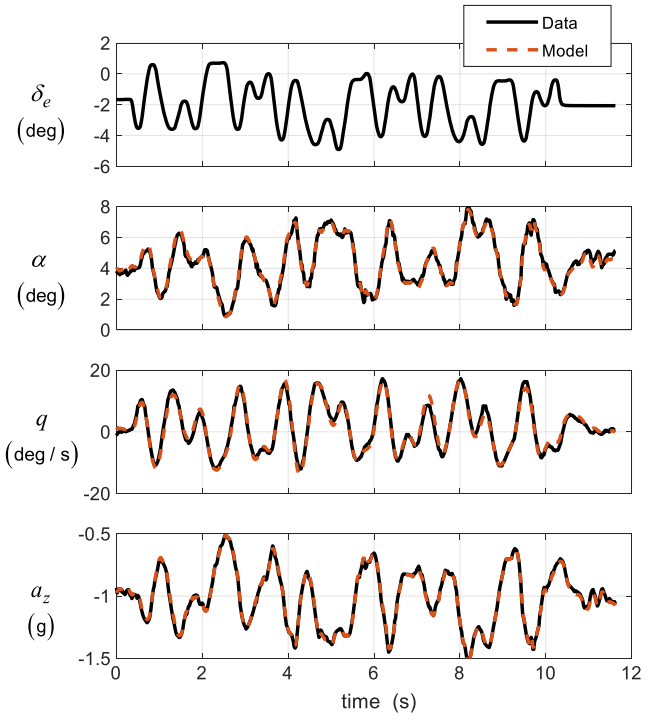

Fig. 11 Filter-error model fit for T-2 flight data in turbulence.

F. Flight Data Corrections

Systematic instrumentation errors in the flight test data used for modeling will degrade modeling accuracy. For example, a scale factor error in the angle-of-attack sensor measurement will cause inaccuracy in the estimate of any model term involving angle of attack. Detailed kinematic relationships and instrumentation error corrections were developed for fixed-wing aircraft [79] and flexible aircraft [80], to produce kinematically consistent data prior to modeling.

Related research produced an approach for real-time data compatibility analysis and systematic instrumentation error correction using output-error parameter estimation in the time domain [81]. Output-error parameter estimation was applied to sequential data windows using a Bayesian formulation to regularize the parameter estimation with modeling results from the preceding data window. This capability can be useful for efficient flight testing and flight safety, as well as real-time fault detection. Although the modeling approach was developed for the real-time data compatibility problem, the method is general and can be applied to other real-time modeling problems as well.

In cases where the inputs are not measured or are measured poorly, a frequency-domain deconvolution method was developed to reconstruct the input data, provided that an accurate dynamic model is available and the data have sufficient signal-to-noise ratio [82]. The approach can be used to reconstruct turbulence inputs, so that conventional modeling methods can be applied for dynamic modeling in turbulence.

G. Model Uncertainty Characterization

Modeling based on measured data is done because the relationships among the measured quantities are unknown. Modeling accuracy will be adversely affected by uncertainties or systematic errors in the data. Consequently, the generally nonlinear effects of errors in the sensor measurements, mass properties, and aircraft geometry on dynamic model accuracy were studied and quantified [83]. This information is important for planning and specifying the flight instrumentation, ground testing, and flight testing necessary to achieve a desired modeling accuracy.

Another important advance was the development of a method for real-time uncertainty estimation for recursive least-squares parameter estimates [84]. Although batch least-squares parameter estimation can be readily converted to a recursive algorithm [5,6], the parameter uncertainty in the batch least-squares algorithm depends on residual characterization using data from the entire maneuver, so that a recursive equivalent is not obvious. The innovation in Ref. [84] was the formulation of a real-time method to characterize generally colored residuals in a sliding data window, and using that result in the parameter uncertainty calculations to properly characterize the uncertainty in recursive least-squares parameter estimates. This advance makes the time-domain recursive least-squares method a good practical option for real-time modeling and fault detection.

Expressions for uncertainty in real-time frequency response estimates using orthogonal optimized multisine inputs were developed and demonstrated in Ref. [34]. This is important for reasons similar to those noted earlier for real-time parameter estimation in the frequency domain and recursive least-squares parameter estimation in the time domain, but also for real-time stability margin estimation and other applications.

When high-resolution analysis frequencies in a partial frequency band are used in the Fourier transform, the parameter uncertainty calculations in the frequency domain must be modified from the conventional expressions. This was first described for the equation-error case in Ref. [49]. More detailed explanations for the modified expression and an extension to output-error parameter estimation in the frequency domain are ongoing work at NASA LaRC.

H. Aeroelastic Modeling Using Distributed Sensing

Another important area of research has been modeling aeroelastic aircraft with distributed sensing. Linear dynamic models for elastic aircraft are of the form

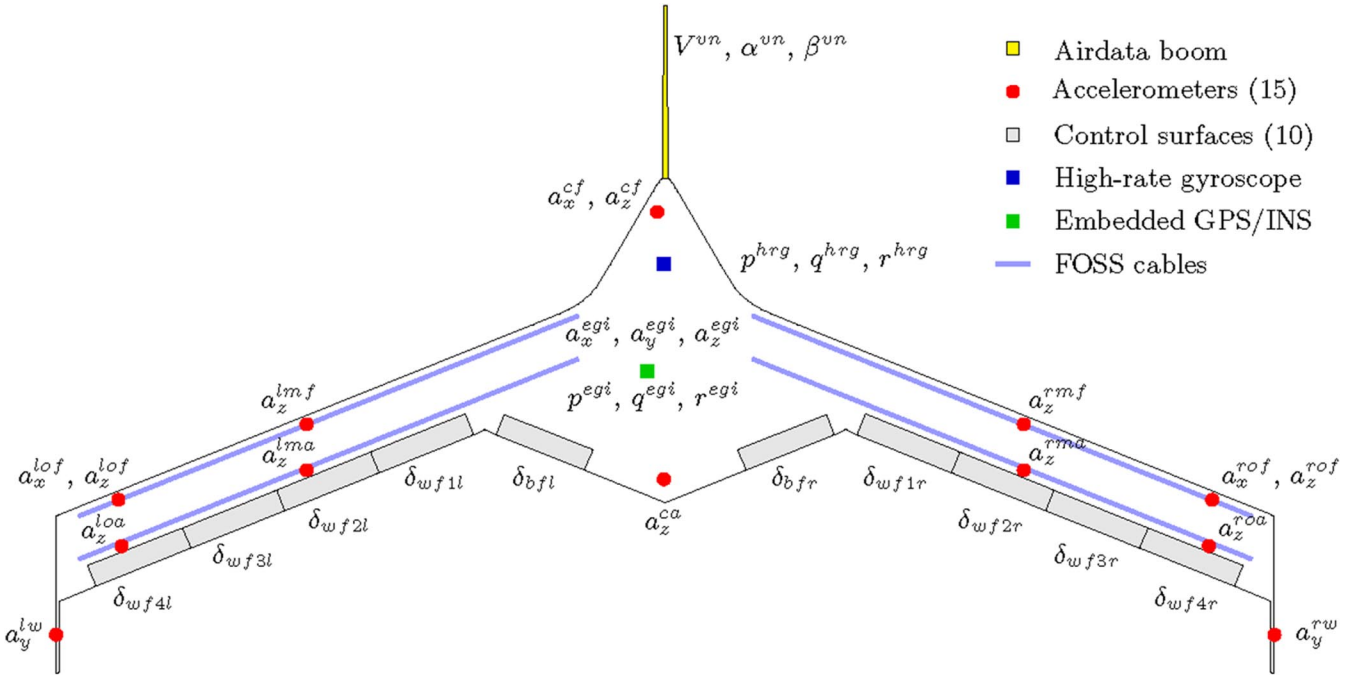

Fig. 12 X-56A distributed sensing for aeroelastic modeling.

$$\begin{bmatrix} \dot{\boldsymbol{x}}_r \\ \dot{\boldsymbol{x}}_e \end{bmatrix} = \begin{bmatrix} \boldsymbol{A}_{rr} & \boldsymbol{A}_{re} \\ \boldsymbol{A}_{er} & \boldsymbol{A}_{ee} \end{bmatrix} \begin{bmatrix} \boldsymbol{x}_r \\ \boldsymbol{x}_e \end{bmatrix} + \begin{bmatrix} \boldsymbol{B}_r \\ \boldsymbol{B}_e \end{bmatrix} \boldsymbol{u} \tag{21a}$$

$$\boldsymbol{y} = \begin{bmatrix} \boldsymbol{C}_r & \boldsymbol{C}_e \end{bmatrix} \begin{bmatrix} \boldsymbol{x}_r \\ \boldsymbol{x}_e \end{bmatrix} + \boldsymbol{D}\boldsymbol{u} \tag{21b}$$

These combine the rigid states $\boldsymbol{x}_r$ with the elastic states $\boldsymbol{x}_e$, which are generalized displacements and velocities for the structural modes. Research with the X-56A airplane showed that the coupling matrices $\boldsymbol{A}_{re}$ and $\boldsymbol{A}_{er}$ were significant and played a role in the flutter instability. Parameter estimation was accomplished using the output error method with Fourier transform data and frequency responses [41,42].

One of the difficulties with flexible aircraft models is that they include flexible modes, which makes the models significantly larger than conventional dynamic models, with more unknown parameters to estimate. This requires more data information and more sensor measurements. Furthermore, the modal states are not directly measured, but rather are observed in linear combinations of measurements from numerous strain gauges and accelerometers distributed over the aircraft. The distributed sensing on the X-56A included 18 accelerometers, 2 gyroscopes, many strain gauges, and 3 fiber-optic strain sensor (FOSS) cables along each wing, as shown in Fig. 12. All of these sensors make the modeling problem much larger and more complex than for conventional aircraft and flight instrumentation.

One approach to alleviate the complexity is to use the redundant sensors to estimate modal states. Explanations of how strain/FOSS measurements and accelerometer measurements can be combined with a finite element model (FEM) to produce estimates of the modal displacements and accelerations can be found in Refs. [29,42]. These data can be combined with kinematic equations of motion in a Kalman filter to improve the modal displacement and acceleration estimates and also admit modal velocity estimates. The equation-error approach can then be used for system identification [29], or these signals can be used for modal control strategies [42].

IV. Future Developments in Aircraft System Identification

Some of the future developments identified in the previous review paper [2] are still valid research directions for aircraft system identification. For example, the use of distributed-parameter models for detailed fluid mechanics and aeroelastic characterization is still a research topic to be explored further. This holds the promise of models that can provide more detailed characterization of the aircraft aerodynamics and structural response, but carries the price of increased data information collection from many sensors, along with the associated data processing and modeling. The X-56A flight research is in this vein, and the future should hold more developments of this kind. Future aircraft such as urban air mobility vehicles will have many control effectors, often using propellers or rotors as control effectors. These aircraft may also employ tilting wings and rotors, which are essentially aircraft configuration changes. Control interaction effects, nonlinearity, and unsteady aerodynamic effects are likely to be significant modeling challenges for these vehicles. Efficient, effective, multi-axis flight test input designs and highly efficient and adaptive modeling techniques will be required.

Major advances have been made in the last 10 years toward the goal of autonomous global aerodynamic modeling in real time onboard the aircraft. With further developments, it is possible to envision aircraft system identification being done autonomously onboard an aircraft in real time on a routine basis, without the need for intervention or judgment from a human analyst. This work will likely continue and has important practical applications for flight testing, simulation development, fault detection, autonomy, and robust adaptive control.

The idea of using a computational fluid dynamics model to substitute for flight testing, sometimes called certification by analysis or virtual flight testing, will also require informative flight test data and aircraft system identification to validate the approach. This is related to the use of distributed parameter models in aircraft system identification. It might be possible to flight-validate distributed-parameter computational methods using distributed sensing and system identification techniques to improve confidence in virtual flight testing.

As in the past, undoubtedly more applications and theoretical problems in aircraft system identification that cannot be foreseen will arise. All vehicles or devices, or even their surrogate computational models, must be tested in the real world at some point. The fundamental activity called system identification, which involves identifying mathematical constructs that characterize measured data from an experiment for purposes of understanding, control, and prediction, will continue to be an essential activity in aerospace engineering.

V. Conclusions

Advances in aircraft system identification at NASA LaRC since 2005 were described, including references to flight test applications and published works. The research advances included flight test experiment design, frequency-domain modeling, real-time autonomous global modeling, rapid simulation development and updating, dynamic modeling in turbulence, flight data corrections, model uncertainty characterization, and aeroelastic modeling using distributed sensing. Software tools for the techniques and investigations discussed in this work, along with many other methods used in aircraft system identification, can be found in the software toolbox called SIDPAC.

Acknowledgments

Research in aircraft system identification was funded by the NASA Hypersonics Program, the NASA Aviation Safety Program, the NASA Vehicle Systems Safety Technologies project, the NASA Aeronautics Mission Directorate, the NASA Fundamental Aeronautics Program, the NASA Learn-to-Fly project, and the NASA Transformational Tools and Technologies project. The efforts of the technical staffs at NASA Langley, NASA Armstrong, NASA Glenn, and the National Test Pilot School in building and testing the aircraft and associated systems, carefully calibrating the instrumentation, and carrying out the flight test operations to collect the high-quality flight data used for the aircraft system identification research described in this work are gratefully acknowledged. Thanks to our many technical colleagues who helped in developing and implementing ideas to solve aircraft system identification problems over the years.

References

[1] Warner, E. P., and Norton, F. H., "Preliminary Report on Free Flight Tests," NACA TR-70, 1919.

[2] Morelli, E. A., and Klein, V., "Application of System Identification to Aircraft at NASA Langley Research Center," *Journal of Aircraft*, Vol. 42, No. 1, Jan.–Feb. 2005, pp. 12–25. https://doi.org/10.2514/1.3648

[3] Gauss, K. F., *Theory of the Motion of the Heavenly Bodies Moving About the Sun in Conic Sections*, a translation of *Theoria Motus* 1809 by Charles Henry Davis, Little, Brown, and Co., Boston, 1857, p. 108.

[4] "System IDentification Programs for AirCraft (SIDPAC)," NASA, https://software.nasa.gov/software/LAR-16100-1 [accessed 11 Jan. 2023].

[5] Klein, V., and Morelli, E. A., *Aircraft System Identification—Theory and Practice*, AIAA Education Series, AIAA, Reston, VA, Aug. 2006, Chaps. 1–12.

[6] Morelli, E. A., and Klein, V., *Aircraft System Identification—Theory and Practice*, 2nd ed., Sunflyte Enterprises, Williamsburg, VA, Dec. 2016, Chaps. 1–12.

[7] Morelli, E. A., "Multiple Input Design for Real-Time Parameter Estimation in the Frequency Domain," *13th IFAC Symposium on System Identification*, Paper REG-360, Aug. 2003. https://doi.org/10.1016/S1474-6670(17)34833-4

[8] Morelli, E. A., "Flight-Test Experiment Design for Characterizing Stability and Control of Hypersonic Vehicles," *Journal of Guidance, Control, and Dynamics*, Vol. 32, No. 3, May–June 2009, pp. 949–959. https://doi.org/10.2514/1.37092

[9] Morelli, E. A., "Flight Test Maneuvers for Efficient Aerodynamic Modeling," *Journal of Aircraft*, Vol. 49, No. 6, Nov.–Dec. 2012, pp. 1857–1867. https://doi.org/10.2514/1.C031699

[10] Morelli, E. A., "Practical Aspects of Multiple-Input Design for Aircraft System Identification Flight Tests," *2021 AIAA Aviation Forum*, AIAA Paper 2021-2795, Aug. 2021. https://doi.org/10.2514/6.2021-2795

[11] Morelli, E. A., Derry, S. D., and Smith, M. S., "Aerodynamic Parameter Estimation for Flight 2 of the X-43A," *Joint Army Navy NASA Air Force (JANNAF) Conference*, Paper No. 20, (SECRET), June 2005.

[12] Morelli, E. A., Derry, S. D., and Smith, M. S., "Aerodynamic Parameter Estimation of the X-43A (Hyper-X) from Flight Test Data," *AIAA Atmospheric Flight Mechanics Conference*, AIAA Paper 2005-5921, Aug. 2005. https://doi.org/10.2514/6.2005-5921

[13] Lechniak, J. A., Rexius, S. L., and Morelli, E. A., "X-51A Scramjet Engine Demonstrator—Waverider Parameter Identification Analysis," 412th Test Wing, 412th Operations Group, Hypersonic Combined Test Force TR 412TW-TIM-13-03, Edwards AFB, CA, March 2014.

[14] Morelli, E. A., Rexius, S. L., and Lechniak, J. A., "Flight Test Experiment Design and Aerodynamic Parameter Estimation for the X-51A Waverider," *20th AIAA International Space Planes and Hypersonic Systems and Technologies Conference*, AIAA Paper 2014-2767, June 2014.

[15] Moes, T., Smith, M., and Morelli, E. A., " 'Excitations for Rapidly Estimating Flight-Control Parameters,' and 'Estimation of Stability and Control Derivatives of an F-15'," *NASA Tech Briefs*, July 2006, pp. 23–24.

[16] Morelli, E. A., and Smith, M. S., "Real-Time Dynamic Modeling—Data Information Requirements and Flight Test Results," *Journal of Aircraft*, Vol. 46, No. 6, Nov.–Dec. 2009, pp. 1894–1905. https://doi.org/10.2514/1.40764

[17] Morelli, E. A., and Cunningham, K., "Aircraft Dynamic Modeling in Turbulence," *AIAA Atmospheric Flight Mechanics Conference*, AIAA Paper 2012-4650, Aug. 2012. https://doi.org/10.2514/6.2012-4650

[18] Morelli, E. A., "Real-Time Aerodynamic Parameter Estimation Without Air Flow Angle Measurements," *Journal of Aircraft*, Vol. 49, No. 4, July–Aug. 2012, pp. 1064–1074. https://doi.org/10.2514/1.C031568

[19] Morelli, E. A., "Dynamic Modeling from Flight Data with Unknown Time Skews," *Journal of Guidance, Control, and Dynamics*, Vol. 40, No. 8, Aug. 2017, pp. 2084–2092. https://doi.org/10.2514/1.G002008

[20] Gingras, D. R., Barnhart, B., Ranaudo, R., Ratvasky, T. P., and Morelli, E. A., "Envelope Protection for In-Flight Ice Contamination," *47th AIAA Aerospace Sciences Meeting*, AIAA Paper 2009-1458, Jan. 2009; also NASA TM-2010-216072, Feb. 2010. https://doi.org/10.2514/6.2009-1458

[21] Ranaudo, R., Martos, B., Norton, B., Gingras, D. R., Barnhart, B., Ratvasky, T. P., and Morelli, E. A., "Piloted Simulation to Evaluate the Utility of a Real Time Envelope Protection System for Mitigating In-Flight Icing Hazards," *AIAA Atmosphere and Space Environments Conference*, AIAA Paper 2010-7987, Aug. 2010; also NASA TM-2011-216951, Oct. 2011. https://doi.org/10.2514/6.2010-7987

[22] Gingras, D. R., Barnhart, B., Ranaudo, R., Martos, B., Ratvasky, T. P., and Morelli, E. A., "Development and Implementation of a Model-Driven Envelope Protection System for In-Flight Ice Contamination," *AIAA Guidance, Navigation, and Control Conference*, AIAA Paper 2010-8141, Aug. 2010; also NASA TM-2011-216960, Oct. 2011. https://doi.org/10.2514/6.2010-8141

[23] Cunningham, K., Foster, J. V., Morelli, E. A., and Murch, A. M., "Practical Application of a Subscale Transport Aircraft for Flight Research in Control Upset and Failure Conditions," *AIAA Atmospheric Flight Mechanics Conference*, AIAA Paper 2008-6200, Aug. 2008. https://doi.org/10.2514/6.2008-6200

[24] Cox, D. E., Cunningham, K., and Jordan, T., "Subscale Flight Testing for Aircraft Loss of Control: Accomplishments and Future Directions," *AIAA Guidance, Navigation, and Control Conference*, AIAA Paper 2012-5029, Aug. 2012. https://doi.org/10.2514/6.2012-5029

[25] Morelli, E. A., "Efficient Global Aerodynamic Modeling from Flight Data," *50th AIAA Aerospace Sciences Meeting*, AIAA Paper 2012-1050, Jan. 2012. https://doi.org/10.2514/6.2012-1050

[26] Morelli, E. A., "Real-Time Global Nonlinear Aerodynamic Modeling for Learn-to-Fly," *2016 AIAA SciTech Forum*, AIAA Paper 2016-2010, Jan. 2016. https://doi.org/10.2514/6.2016-2010

[27] Morelli, E. A., "Practical Aspects of Real-Time Modeling for the Learn-To-Fly Concept," *Atmospheric Flight Mechanics Conference, 2018 AIAA Aviation Forum*, AIAA Paper 2018-3309, June 2018. https://doi.org/10.2514/6.2018-3309

[28] Morelli, E. A., "Autonomous Real-Time Global Aerodynamic Modeling in the Frequency Domain," *2020 AIAA SciTech Forum*, AIAA Paper 2020-0761, Jan. 2020. https://doi.org/10.2514/6.2020-0761

[29] Grauer, J. A., and Boucher, M. J., "Real-Time System Identification of Flexible Aircraft," *AIAA Atmospheric Flight Mechanics Conference*, AIAA Paper 2018-3155, June 2018. https://doi.org/10.2514/6.2018-3155

[30] Grauer, J. A., and Boucher, M. J., "Real-Time Estimation of Bare-Airframe Frequency Responses from Closed-Loop Data and Multisine Inputs," *Journal of Guidance, Control, and Dynamics*, Vol. 43, No. 2, Feb. 2020, pp. 288–298. https://doi.org/10.2514/1.G004574

[31] Grauer, J. A., "Frequency Response Estimation for Multiple Aircraft Control Loops Using Orthogonal Phase-Optimized Multisine Inputs," *MDPI Processes*, Vol. 10, No. 4, March 2022, pp. 1–24. https://doi.org/10.3390/pr10040619

[32] Grauer, J. A., Morelli, E. A., and Murri, D. G., "Flight Test Techniques for Quantifying Pitch Rate and Angle of Attack Rate Dependencies," *Journal of Aircraft*, Vol. 54, No. 6, Nov.–Dec. 2017, pp. 2367–2377. https://doi.org/10.2514/1.C034407

[33] Holzel, M. S., and Morelli, E. A., "Real-Time Frequency Response Estimation from Flight Data," *Journal of Guidance, Control, and Dynamics*, Vol. 35, No. 5, Sept.–Oct. 2012, pp. 1406–1417. https://doi.org/10.2514/1.56782

[34] Grauer, J. A., and Morelli, E. A., "Method for Real-Time Frequency Response and Uncertainty Estimation," *Journal of Guidance, Control, and Dynamics*, Vol. 37, No. 1, Jan.–Feb. 2014, pp. 336–344. https://doi.org/10.2514/1.60795

[35] Tischler, M. B., Ivler, C. M., and Berger, T., "Comment on 'Method for Real-Time Frequency Response and Uncertainty Estimation'," *Journal of Guidance, Control, and Dynamics*, Vol. 38, No. 3, March 2015, pp. 547–549. https://doi.org/10.2514/1.G000780

[36] Grauer, J. A., and Morelli, E. A., "Reply by the Authors to M. Tischler, C. Ivler, and T. Berger," *Journal of Guidance, Control, and Dynamics*, Vol. 38, No. 3, March 2015, pp. 549–550. https://doi.org/10.2514/1.G001090

[37] Grauer, J. A., "Dynamic Modeling Using Output-Error Parameter Estimation based on Frequency Responses Estimated with Multisine Inputs," NASA TM-2018-220108, Nov. 2018.

[38] Grauer, J. A., and Boucher, M. J., "Aircraft System Identification from Multisine Inputs and Frequency Responses," *Journal of Guidance, Control, and Dynamics*, Vol. 43, No. 12, Dec. 2020, pp. 2391–2398. https://doi.org/10.2514/1.G005131

[39] Grauer, J. A., "Aircraft Fault Detection Using Real-Time Frequency Response Estimation," *AIAA Guidance, Navigation, and Control Conference*, AIAA Paper 2016-0372, Jan. 2016. https://doi.org/10.2514/6.2016-0372

[40] Grauer, J. A., and Boucher, M. J., "Aeroelastic Modeling of X-56A Stiff-Wing Configuration Flight Test Data," *AIAA Atmospheric Flight Mechanics Conference*, AIAA Paper 2017-0699, Jan. 2017. https://doi.org/10.2514/6.2017-0699

[41] Grauer, J. A., and Boucher, M. J., "Identification of Aeroelastic Models for the X-56A Longitudinal Dynamics Using Multisine Inputs and Output Error in the Frequency Domain," *MDPI Aerospace*, Vol. 6, No. 2, Feb. 2019, Paper 24, pp. 1–25. https://doi.org/10.3390/aerospace6020024

[42] Grauer, J. A., and Boucher, M. J., "System Identification of Flexible Aircraft: Lessons Learned from the X-56A Phase 1 Flight Tests," *AIAA Atmospheric Flight Mechanics Conference*, AIAA Paper 2020-1017, Jan. 2020. https://doi.org/10.2514/6.2020-1017

[43] Morelli, E. A., "Determining Aircraft Moments of Inertia from Flight Test Data," *Journal of Guidance, Control, and Dynamics*, Vol. 45, No. 1, Jan. 2022, pp. 4–14. https://doi.org/10.2514/1.G006072

[44] Morelli, E. A., "Subsonic Flight Test Maneuver Design and Aerodynamic Modeling for the Dream Chaser Space Vehicle," NASA TM-2019-220261, March 2019.

[45] Brandon, J. M., Derry, S. D., Heim, E. H., Hueschen, R. M., and Bacon, B. J., "Ares-I-X Stability and Control Flight Test: Analysis and Plans," *AIAA SPACE 2008 Conference & Exposition*, AIAA Paper 2008-7807, Sept. 2008. https://doi.org/10.2514/6.2008-7807

[46] Derry, S. D., "Ares I-X Flight Test Overview and System ID Results," *106th SAE/IEEE Aerospace Control and Guidance Systems Committee (ACGSC) Meeting*, Oct. 2010.

[47] Derry, S. D., "Ares I-X Flight Test System Identification Results," *58th JANNAF Propulsion Meeting*, April 2011.

[48] Morelli, E. A., "Optimal Input Design for Aircraft Stability and Control Flight Testing," *Journal of Optimization Theory and Applications, Special Issue: Optimization Theory and Application to Aerospace Systems*, Vol. 191, No. 2–3, Dec. 2021, pp. 415–439. https://doi.org/10.1007/s10957-021-01912-0

[49] Morelli, E. A., and Grauer, J. A., "Practical Aspects of Frequency-Domain Approaches for Aircraft System Identification," *Journal of Aircraft*, Vol. 57, No. 2, March–April 2020, pp. 268–291. https://doi.org/10.2514/1.C035599

[50] Lanczos, C., *Applied Analysis*, Dover, New York, 1988, pp. 331–344.

[51] Grauer, J. A., "Random Noise Generation Using Fourier Series," *Journal of Aircraft*, Vol. 55, No. 4, July–Aug. 2018, pp. 1753–1759. https://doi.org/10.2514/1.C034616

[52] Grauer, J. A., "A Comparison of Three Random Number Generators for Aircraft Dynamic Modeling Applications," NASA TM-2017-219612, May 2017.

[53] Grauer, J. A., "In-Flight Turbulence Emulation for Fixed-Wing Aircraft Using Equivalent Multisine Excitations," NASA TM-20210020347, Sept. 2021.

[54] Martos, B., and Noriega, A., "A Method for Real-Time Pilot Modeling and Multisine Tracking Input Design," *2019 AIAA SciTech Forum*, AIAA Paper 2019-1318, Jan. 2019. https://doi.org/10.2514/6.2019-1318

[55] Brandon, J. M., and Morelli, E. A., "Nonlinear Aerodynamic Modeling From Flight Data Using Advanced Piloted Maneuvers and Fuzzy Logic," NASA TM-2012-217778, Oct. 2012.

[56] Morelli, E. A., Cunningham, K., and Hill, M. A., "Global Aerodynamic Modeling for Stall/Upset Recovery Training Using Efficient Piloted Flight Test Techniques," *AIAA Modeling and Simulation Technologies Conference*, AIAA Paper 2013-4976, Aug. 2013. https://doi.org/10.2514/6.2013-4976

[57] Grauer, J. A., and Martos, B., "Evaluation of Piloted Inputs for Onboard Frequency Response Estimation," *AIAA Atmospheric Flight Mechanics Conference*, AIAA Paper 2013-4921, Aug. 2013. https://doi.org/10.2514/6.2013-4921

[58] Brandon, J. M., and Morelli, E. A., "Real-Time Global Nonlinear Aerodynamic Modeling from Flight Data," *Journal of Aircraft*, Vol. 53, No. 5, Sept.–Oct. 2016, pp. 1261–1297. https://doi.org/10.2514/1.C033133

[59] Klein, V., "Aircraft Parameter Estimation in Frequency Domain," *AIAA Atmospheric Flight Mechanics Conference*, AIAA Paper 1978-1344, Aug. 1978. https://doi.org/10.2514/6.1978-1344

[60] Klein, V., "Maximum Likelihood Method for Estimating Airplane Stability and Control Parameters from Flight Data in Frequency Domain," NASA TP-1637, May 1980.

[61] Klein, V., "Estimation of Aircraft Aerodynamic Parameters from Flight Data," *Progress in Aerospace Sciences*, Vol. 26, No. 1, 1989, pp. 1–77. https://doi.org/10.1016/0376-0421(89)90002-X

[62] Morelli, E. A., "Practical Aspects of the Equation-Error Method for Aircraft Parameter Estimation," *AIAA Atmospheric Flight Mechanics Conference*, AIAA Paper 2006-6144, Aug. 2006. https://doi.org/10.2514/6.2006-6144

[63] Morelli, E. A., "Real-Time Parameter Estimation in the Frequency Domain," *Journal of Guidance, Control, and Dynamics*, Vol. 23, No. 5, Sept.–Oct. 2000, pp. 812–818. https://doi.org/10.2514/2.4642

[64] Morelli, E. A., and Cooper, J., "Frequency-Domain Method for Automated Simulation Updates Based on Flight Data," *Journal of Aircraft*, Vol. 52, No. 6, Nov.–Dec. 2015, pp. 1995–2008. https://doi.org/10.2514/1.C033121

[65] Grauer, J. A., Heeg, J., and Morelli, E. A., "Real-Time Frequency Response Estimation of Joined-Wing SensorCraft Aeroelastic Wind Tunnel Data," *AIAA Atmospheric Flight Mechanics Conference*, AIAA Paper 2012-4641, Aug. 2012. https://doi.org/10.2514/6.2012-4641

[66] Tischler, M. B., and Remple, R. K., *Aircraft and Rotorcraft System Identification—Engineering Methods with Flight Test Examples*, 2nd ed., AIAA Education Series, AIAA, Reston, VA, 2012.

[67] Berger, T., Tischler, M. B., Knapp, M. E., and Lopez, M. J. S., "Identification of Multi-Input Systems in the Presence of Highly Correlated Inputs," *Journal of Guidance, Control, and Dynamics*, Vol. 41, No. 10, Oct. 2018, pp. 2247–2257. https://doi.org/10.2514/1.G003530

[68] Heim, E. H. D., Viken, E. M., Brandon, J. M., and Croom, M. A., "NASA's Learn-to-Fly Project Overview," *Atmospheric Flight Mechanics Conference, 2018 AIAA Aviation Forum*, AIAA Paper 2018-3307, June 2018. https://doi.org/10.2514/6.2018-3307

[69] Simmons, B. M., Morelli, E. A., Busan, R. C., Hahne, D. B., and O'Neal, A. W., "Aero–Propulsive Modeling for eVTOL Aircraft Using Wind Tunnel Testing with Multisine Inputs," *2022 AIAA Aviation Forum*, AIAA Paper 2022-3603, June 2022. https://doi.org/10.2514/6.2022-3603

[70] Grauer, J. A., and Morelli, E. A., "A Generic Global Aerodynamic Model for Aircraft," *Journal of Aircraft*, Vol. 52, No. 1, Jan.–Feb. 2015, pp. 13–20. https://doi.org/10.2514/1.C032888

[71] Morelli, E. A., and Ward, D. G., "Automated Simulation Updates based on Flight Data," *AIAA Atmospheric Flight Mechanics Conference*, AIAA Paper 2007-6714, Aug. 2007. https://doi.org/10.2514/6.2007-6714

[72] Brian, G., and Morelli, E. A., "Rapid Automated Aircraft Simulation Model Updating From Flight Data," *Fourteenth Australian International Aerospace Congress*, Royal Aeronautical Soc., Melbourne, Australia, March 2011, pp. 430–439.

[73] Martos, B., and Morelli, E. A., "Using Indirect Turbulence Measurements for Real-Time Parameter Estimation in Turbulent Air," *AIAA Atmospheric Flight Mechanics Conference*, AIAA Paper 2012-4651, Aug. 2012. https://doi.org/10.2514/6.2012-4651

[74] Grauer, J. A., "Aerodynamic Parameter Estimation Using Reconstructed Turbulence Measurements," *Journal of Aircraft*, Vol. 58, No. 5, Sept.–Oct. 2021, pp. 1022–1033. https://doi.org/10.2514/1.C035933

[75] Maine, R. E., and Iliff, K. W., "Formulation and Implementation of a Practical Algorithm for Parameter Estimation with Process and Measurement Noise," *SIAM Journal of Applied Mathematics*, Vol. 41, No. 3, 1981, pp. 558–579. https://doi.org/10.1137/0141045

[76] Grauer, J. A., and Morelli, E. A., "A New Formulation of the Filter-Error Method for Aerodynamic Parameter Estimation in Turbulence," *2015 AIAA Aviation Forum*, AIAA Paper 2015-2704, June 2015. https://doi.org/10.2514/6.2015-2704

[77] Morelli, E. A., "Estimating Noise Characteristics from Flight Test Data Using Optimal Fourier Smoothing," *Journal of Aircraft*, Vol. 32, No. 4, July–Aug. 1995, pp. 689–C. https://doi.org/10.2514/3.46778

[78] Miller, L. J., Grauer, J. A., Pei, J., and Nelson, S. L., "Reconstruction of the Apollo 11 Moon Landing Final Descent Trajectory," NASA TM-20220007267, Aug. 2022.

[79] Grauer, J. A., "Position Corrections for Airspeed and Flow Angle Measurements on Fixed-Wing Aircraft," NASA TM-2017-219795, Nov. 2017.

[80] Grauer, J. A., and Boucher, M. J., "Output Measurement Equations for Flexible Aircraft Flight Dynamics," NASA TM-2018-220102, Oct. 2018.

[81] Grauer, J. A., "Real-Time Data Compatibility Analysis Using Output-Error Parameter Estimation," *Journal of Aircraft*, Vol. 52, No. 3, May–June 2015, pp. 940–947. https://doi.org/10.2514/1.C033182

[82] Grauer, J. A., and Boucher, M. J., "Frequency-Domain Deconvolution for Aerospace Applications," *AIAA Atmospheric Flight Mechanics Conference*, AIAA Paper 2018-3157, June 2018. https://doi.org/10.2514/6.2018-3157

[83] Grauer, J. A., and Morelli, E. A., "Dependence of Dynamic Modeling Accuracy on Sensor Measurements, Mass Properties, and Aircraft Geometry," NASA TM-2013-218056, Nov. 2013.

[84] Grauer, J. A., and Morelli, E. A., "Parameter Covariance for Aircraft Aerodynamic Modeling Using Recursive Least Squares," *2016 AIAA SciTech Forum*, AIAA Paper 2016-2009, Jan. 2016. https://doi.org/10.2514/6.2016-2009